presence of APV, at least a 4-min "rest" interval was interposed between separate episodes of high-frequency stimulation to avoid changes in the responses [53]. Picrotoxin (PiTX) was dissolved in ethanol to make a 50-mM stock solution. The low Ca^{2+} aCSF had the following ion concentrations: 124 mM NaCl, 2.5 mM KCl, 0.25 mM $CaCl_2$, 4 mM $MgCl_2$, 2 mM $MgSO_4$, 1.25 mM NaH_2PO_4, 26 mM $NaHCO_3$, and 10 mM glucose, pH 7.4. Other common reagents were obtained through local resellers in Japan.

When there was a significant difference between groups, Tukey's multiple comparison test was performed to determine the levels of significance on IgorPro software. All the measurements are presented as mean±SEM, and *n* means the number of slices tested unless otherwise stated.

Results

Tetanic stimulation (100 Hz)-induced progressive decrease in EPSPs measured using optical signals

High-frequency (100 Hz) tetanic burst stimulation applied to the middle of the SR of CA1 typically elicited a long-lasting depolarizing optical signal [55] (for a video of these optical recordings under normal conditions, please see Supplemental movie s1.mpg). Optical signals obtained from the SR indicated a tetanus-induced long-lasting depolarizing response on which individual responses, i.e., EPSPs, to individual stimulation pulses were superimposed (black trace in Fig. 1b). On measuring the height of each peak amplitude from the bottom of the inter-EPSP response, we observed that the amplitude of individual EPSPs appeared to decrease.

For a more detailed study of the progressive decrease, we attempted to separate the individual EPSPs from the long-lasting depolarizing component. A profile drawn tangent to the wave troughs between individual responses should provide a fair representation of the time course of the long-lasting depolarization. Hence, we chose the minimum peak between each response as the representative data for the fit of a long-lasting depolarization. We started with the simplest single exponential equation:

$$f(t) = a(1 - \exp(-t/\tau)) \qquad (1)$$

where a is the maximum amplitude of the response and τ is the time constant. Since the data points in the first 200 ms appeared to contain a component that would not fit in Eq. 1, we excluded these data points. The resulting fit is shown as a blue line in Fig. 1b. The subtraction of this curve from the data representing the optical signal is shown in Fig. 1c as a black trace (please also see Supplemental movie s2.mpg). The subtracted trace (black trace in Fig. 1c) shows that the amplitudes of individual responses in this residual potential decreased with increasing number of tetanic stimuli, suggesting that EPSPs incrementally decreased in accordance with tetanic stimulation. The amplitude of the optical signal to the first stimulation was significantly larger than that to the last (40th) stimulation (first stimulation, $4.04 \times 10^{-3} \pm 0.66 \times 10^{-3}$; 40th stimulation, $0.75 \times 10^{-3} \pm 0.09 \times 10^{-3}$; n=7; P<0.001; the optical signal was measured at 200 μm from the stimulation site). The fitted amplitude of the long-lasting depolarization (a) was the largest near the stimulating electrode and decreased at points located away from the stimulating electrode. The time constant (t) was approximately 480 ms for EPSPs recorded

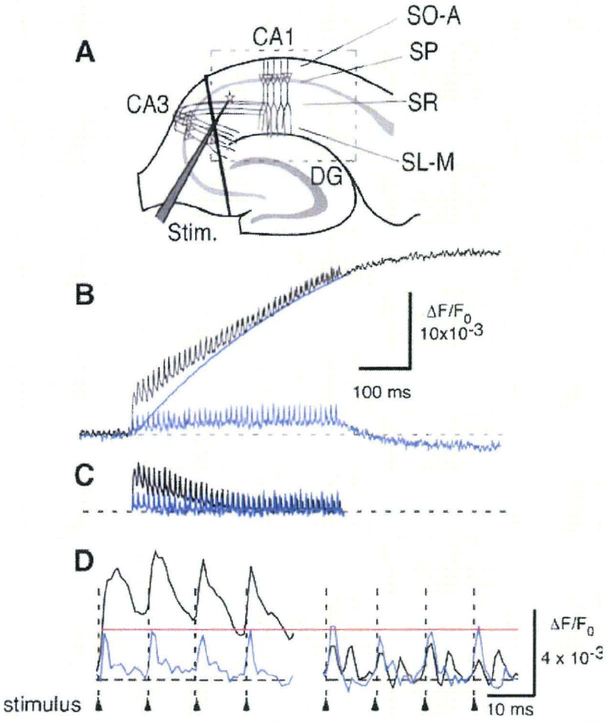

Fig. 1 Progressive decrease in EPSPs during tetanic stimulation. **a** A schematic of hippocampal slice preparation and the field of view of the imaging system (*dashed square*). *SO-A* stratum oriens–alveus, *SP* stratum pyramidale, *SR* stratum radiatum, *SL-M* stratum lacunosum–moleculare. **b** The *black line* is a representative trace of the optical signal obtained at a pixel in the middle of the stratum radiatum in the CA1 region in response to tetanic stimulation (100 Hz, 40 pulses; see also Supplemental movie s1.mpg), and the *blue line* is a trace of the optical signals obtained using aCSF with a low Ca^{2+} content. This aCSF contained 0.25 mM Ca^{2+} and 6 mM Mg^{2+}. The smooth *blue line* represents the curve resulting from single exponential fit of the data (see "Results" section for more details). **c** The residual curve resulting from the subtraction of the smooth blue line from data representing the optical signals shown in **b** is superimposed on the response obtained using the aCSF with a low Ca^{2+} content (*blue trace*). **d** The traces in **c** are displayed together with expanded time and amplitude scales; these have been taken from the initial (*left*) and final phases (*right*) of tetanic stimulation. The timings for stimulation are indicated at the *bottom of the figure* (*arrowheads*). The *red horizontal line* indicates the amplitude of the fast transient response in the low Ca^{2+} content solution; the amplitude of the fast transient did not change during tetanus

around the stimulating electrode and decreased to 200 ms at the farthest point from the electrode.

The optical signal consisted of the postsynaptic membrane potential response from a population of pyramidal cells and the population presynaptic fiber activity. We noticed that the small fast components corresponding to each stimulus were superimposed on the long-lasting depolarization and thought that this could be attributable to presynaptic fiber activity. In order to investigate whether presynaptic fiber activity is responsible for the small fast components that crown the long-lasting slower depolarization and correspond to each stimulus, we repeated these experiments after suppressing synaptic transmission by a low Ca^{2+} aCSF. Most of the long-lasting component was absent when the perfusate contained reduced levels of Ca^{2+} (blue trace in Fig. 1b); the amplitude of the residual fast transient responses did not change during tetanus. The fast transient responses were sensitive to tetrodotoxin, except in the close vicinity of the stimulating electrode; therefore, we conclude that these responses can be attributed to presynaptic fiber activity. The responses recorded in aCSF with a low Ca^{2+} content (blue traces) and the subtracted response (black trace) have been compared in Fig. 1c. The traces from the initial (left) and final phases of the tetanus (right) are displayed with expanded time and amplitude scales in Fig. 1d. The amplitude of the fast transient response in aCSF with a low Ca^{2+} content did not change during the tetanus (first stimulation, $1.21 \times 10^{-3} \pm 0.48 \times 10^{-3}$; 40th stimulation, $1.11 \times 10^{-3} \pm 0.36 \times 10^{-3}$; $n=3$). The amplitude of the fast transient response, which corresponds to presynaptic fiber activity, is indicated by the horizontal red line. The subtracted signal amplitude (black trace) during the initial phase was larger than the fast transient response, whereas the signal amplitude during the last phase showed two peaks for each stimulation (arrowheads under the traces). The latter peak, which should correspond to the EPSP, was smaller than the fast transient response (red line). The fast presynaptic activities of the subtracted trace were similar to those measured in low Ca^{2+} solution after the initiation of fitting, i.e., after 200 ms from the initiation of tetanic stimulation; therefore, we can postulate that the observed decrease in the later individual EPSP components in the subtracted trace may correspond to the progressive decrease in EPSPs.

Progressive decrease of EPSPs and EPSCs during high-frequency tetanic stimulation

To confirm that the progressive decrease is not an artifact of the optical-recording technique, electrophysiological responses corresponding to the same stimulation were also examined (Fig. 2). High-frequency stimulation produced repetitive fEPSPs recorded from the middle of CA1 SR (Fig. 2a). The individual responses were superimposed on a slow negative potential shift lasting about 1 s. The amplitude of the individual responses seemed to gradually decrease with increase in the number of afferent shocks, as shown in the time-expanded scale (Fig. 2b). That is, the amplitude of the first response (closed arrow) was significantly larger than that of the last response (red colored; open arrow; −1.02±0.23 mV to the first stimulation, −0.34±0.08 mV to the 40th stimulation, $P<0.05$, $n=5$). For comparison, the response to the 40th stimulus was highlighted in red and was also superimposed on the first response in Fig. 2b. It was obvious that the last response consisted of two peaks. This can be interpreted to reflect the fiber volley caused by presynaptic fiber activity and the fEPSP, as was similarly observed in the optical signal in Fig. 1d. That is, fEPSP amplitude progressively decreased, while the presynaptic fiber volleys were preserved. This corresponds to the two peaks observed in the optical signal shown in Fig. 1d.

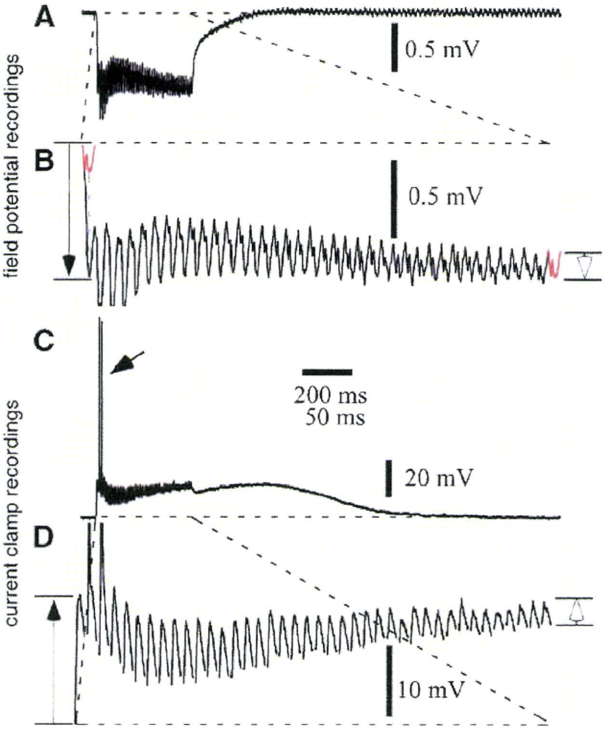

Fig. 2 Progressive decrease of excitatory postsynaptic potentials (EPSPs) in response to tetanic stimulation (100 Hz, 40 pulses) and field potentials (fEPSPs) in rat hippocampal CA1 slices. **a**, **b** Field potential recording. Representative field potential changes in response to the tetanic stimulation; recorded with an extracellular electrode positioned in the middle of stratum radiatum (about 200 μm from stratum pyramidale, 400 μm from stimulating electrode) of the slice. The response to the last stimulus was highlighted in *red color* and was also superimposed in the first response in trace **b**. A *blue dashed line at the first response* shows the timing of the peaks. **c**, **d** Representative trace of membrane potential responses recorded under current clamp. There are two APs at the beginning of the tetanic stimulation (*arrow*). These APs are truncated in **d**. *Bottom ticks* illustrate the timing of the stimulation pulses. Traces were acquired in the presence of 50 μM of APV in the perfusate (see "Materials and methods" section)

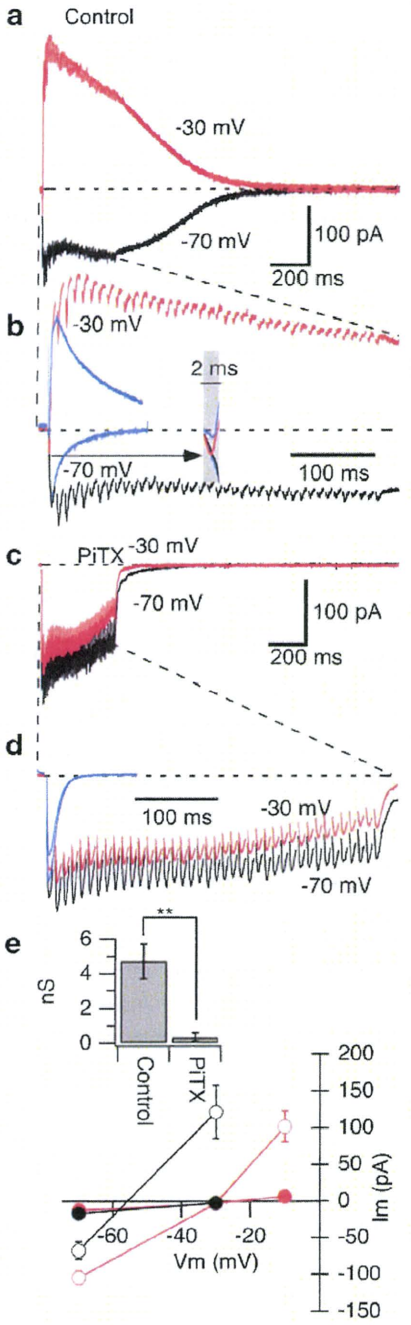

Fig. 3 Incremental inhibition of EPSC components with a depolarized holding potential (**a**, **b**) and in the presence of the $GABA_A$ receptor antagonist PiTX (**c**, **d**); recorded with $Cs\text{-}MeSO_3$-based, low Cl^- internal pipette solution. **a**, **b** Representative membrane current response to tetanic stimulation superimposed on responses to a single stimulation (*blue traces*). Holding potential was −70 mV (*black traces*) and −30 mV (*red traces*) for each case. Time expanded traces of the first part (gray) are superimposed in **b** middle. **c**, **d** Representative membrane current responses in the presence of PiTX. **e** Current–voltage relationships of the long-lasting tail components measured at 50 ms from the cessation of stimulus train in the control (*open circle*) and PiTX (*close circle*) condition recorded with low Cl^- pipette internal solution ($E_{Cl}=-73$ mV, *black symbols*) and higher Cl^- pipette internal solution ($E_{Cl}=-29$ mV, *red symbols*). Conductance calculated from the current–voltage relationships with low Cl^- solution are plotted in the *inset of the graph*. $^{**}P<0.01$. *Error bars*, SEM. $n=5$

To find out whether the progressive decrease can be seen on a single cell level, the response was tested under current clamp conditions with a potassium-based internal pipette solution. The membrane potential showed a repetitive, transient depolarizing response (corresponding to EPSPs), sometimes followed by action potentials. The latter occurred especially during the early phase of stimulation. Two action potentials are observed in the early phase of stimulation (Fig. 2c, arrow). During high-frequency stimulation, the baseline response showed a sustained, depolarizing membrane potential shift. This sustained depolarization decayed slowly toward the resting potential within a few hundreds of milliseconds after cessation of stimulation. However, sometimes it was followed by a gradual rise and a peak after a few tens of milliseconds from the end of stimulation, again slowly decaying to the resting level within a few seconds (see, for example, Fig. 1b of Tominaga et al. [55], which shows a membrane potential trace obtained with a sharp intracellular electrode). The apparent amplitude of the individual transient responses to each shock decreased with increase in the number of shocks (cf. closed arrow and open arrow in Fig. 2d; 12.97± 4.61 mV to the first stimulation, 4.61±1.35 mV to the 40th stimulation; $P<0.05$, $n=4$). This corroborates the effect observed in optical recordings in that EPSP amplitude incrementally decreases in terms of electrophysiological recording as recorded under current clamp conditions.

To determine whether the decrease in membrane potential response was caused by decreased synaptic transmission, we examined membrane current responses under voltage-clamp conditions with Cs-based, low Cl^- internal pipette solution ($E_{Cl}=-73$ mV; Fig. 3). Please note that the reversal potential of $GABA_A$ receptors should be more positive than the E_{Cl} due to the possible contribution of other ion species such as HCO_3^-. The EPSCs showed progressive decrease (Fig. 3a). EPSC to the first stimulation was significantly larger than that to the last stimulation (−95.98± 15.21 pA to the first stimulation, −10.82±1.07 pA to the 40th stimulation at −70 mV, $P<0.001$, $n=5$, n means number of cells). $GABA_A$ receptor antagonists reduce the amplitude of high-frequency stimulation-induced long-lasting depolarization [27, 44, 51, 53]. The long-lasting component of the current reversed its sign when the holding potential was brought to −30 from −70 mV (Fig. 3a, b; red and black trace, respectively). EPSCs superimposed on the long-lasting components also showed a progressive decrease in amplitude at depolarized holding potentials (−43.03±−1.16 pA to the first stimulation, −5.41±1.56 pA to the 40th stimulation at −30 mV, $P<0.01$, $n=5$ cells). That is, the progressive decrease shown in membrane potential changes, i.e., EPSP, are accompanied by a reduction in EPSC amplitudes.

Application of PiTX reduced the long-lasting tail current components (Fig. 3c, d), and the current did not show a reversal, even when the holding potential was brought to −30 mV. The amplitude of the long-lasting tail current components (50 ms after cessation of the stimulation train) was plotted in Fig. 3e. The slope conductance calculated from these values was significantly different between control and PiTX application (4.73±0.99 nS in control, 0.36± 0.25 nS in PiTX, n=5, P<0.01, n means number of cells). The reversal potential of the tail current recorded with the low Cl^- internal solution (black symbols in Fig. 3e) was shifted in positive direction if we used an internal solution with higher Cl^- concentration (E_{Cl}=−29 mV). This observation supports the idea that the tail current components are primarily carried by Cl^-.

The individual EPSCs were not clearly distinguishable due to their longer duration in Fig. 3c. However, EPSCs did not show the progressive decrease as was observed under control condition (cf. Fig. 3b, d). We thought that the peak amplitude of EPSCs did not change during the period of burst stimulation so that the envelope of the response appeared to be square (Fig. 3c), even when the long-lasting tail was suppressed under PiTX. These results suggest that PiTX diminished the progressive decrease of EPSC.

Recovery of individual responses from incremental inhibition

During the tetanic stimulation, individual EPSPs are difficult to be isolated; hence, to study the progressive decrease of EPSPs clearer, we examined the recovery of EPSP amplitudes by probing with a single stimulus at various times after cessation of the standard tetanic stimulation. We probed the EPSP amplitude at 20, 50, 100, 200, and 500 ms after the tetanus ended, as shown in Fig. 4a. These single probe stimuli elicited responses (blue rectangular highlights) superimposed on the tail of the long-lasting depolarizing optical signal and on the long tail of the field potential shift (Fig. 4b, bottom).

The traces shown in Fig. 4c show the time course of incremental inhibition of EPSPs during tetanic stimulation and their recovery as a function of time from the beginning of the stimulation protocol; the long-lasting depolarizing component was subtracted out, as before. The amplitude of probe stimulus was significantly smaller than the control when the delay was smaller than 200 ms (delay <50 ms, P< 0.001; delay 100 ms, P<0.05 at 100 μm away from the stimulation site). The pooled data are shown in Fig. 4f.

The time course of the recovery in presence of PiTX was tested using the same probe stimuli (Fig. 4d). Since the individual EPSP was not isolated under PiTX, a trace during the tetanic stimulation is shown in Fig. 4e. The response amplitudes to the delayed probe stimuli were somewhat smaller than the initial amplitude of the high-frequency responses (thin blue horizontal line; a and b in Fig. 4d), but they recovered soon (c in Fig. 4d). There were no significant differences in the amplitude of the response to the delayed probe stimuli compared to the control.

Figure 4f shows the pooled data of the amplitude of the probe signals relative to the control signal at different distances from the stimulation site in the control and in the presence of PiTX. In the control condition, the amplitude of the probe signals in the vicinity of the stimulation electrode (100 to 300 μm) was suppressed. The decreased response gradually recovered to the original level. In contrast, the response at distal areas (600 to 900 μm) showed significant transient facilitation after cessation of the tetanic stimulation. The distance-dependent decrease and facilitation of EPSPs was diminished by the application of PiTX. This finding is apparent in the three-dimensional plot shown in Fig. 4g. This can also be seen in the traces shown in Figs. 6a (control) and 7a (in the presence of PiTX).

Inhibition of the long-lasting $GABA_A$-dependent component and the relative insensitivity of the EPSP response amplitudes to delayed posttetanus probe stimuli suggests that the $GABA_A$ antagonist PiTX also reversed, at least partially, the incremental inhibition of EPSPs.

Spatial convergence of the response and effect of PiTX on spatial convergence

The progressive decrease in EPSPs is one of the characteristics of tetanic burst stimulation-induced responses. A steep spatial dependence of the long-lasting depolarizing response amplitude is another characteristic [55]. In order to study the GABA-mediated modulation of depolarizing transmission and propagation in area CA1, we examined the spatial convergence of the response under standard conditions (control) and in the presence of PiTX.

The peak amplitude of the responses to tetanic stimulation in slices bathed in normal aCSF (control) and in aCSF containing PiTX is plotted as three-dimensional graphs in Fig. 5a. The response was only weakly convergent in the presence of PiTX. This difference is clearer in Fig. 5b, in which the two plots are re-color-coded and superimposed. The steep convergence of the response at the site of stimulation in the control condition (grayscale) was mostly absent when $GABA_A$ receptors were pharmacologically antagonized, while the response amplitude in the distal parts of CA1 was fairly similar in the two conditions.

Representative traces showing the effect of PiTX on the optical signals at different pixels in SR are shown in Fig. 5c. The long-lasting depolarizing component was

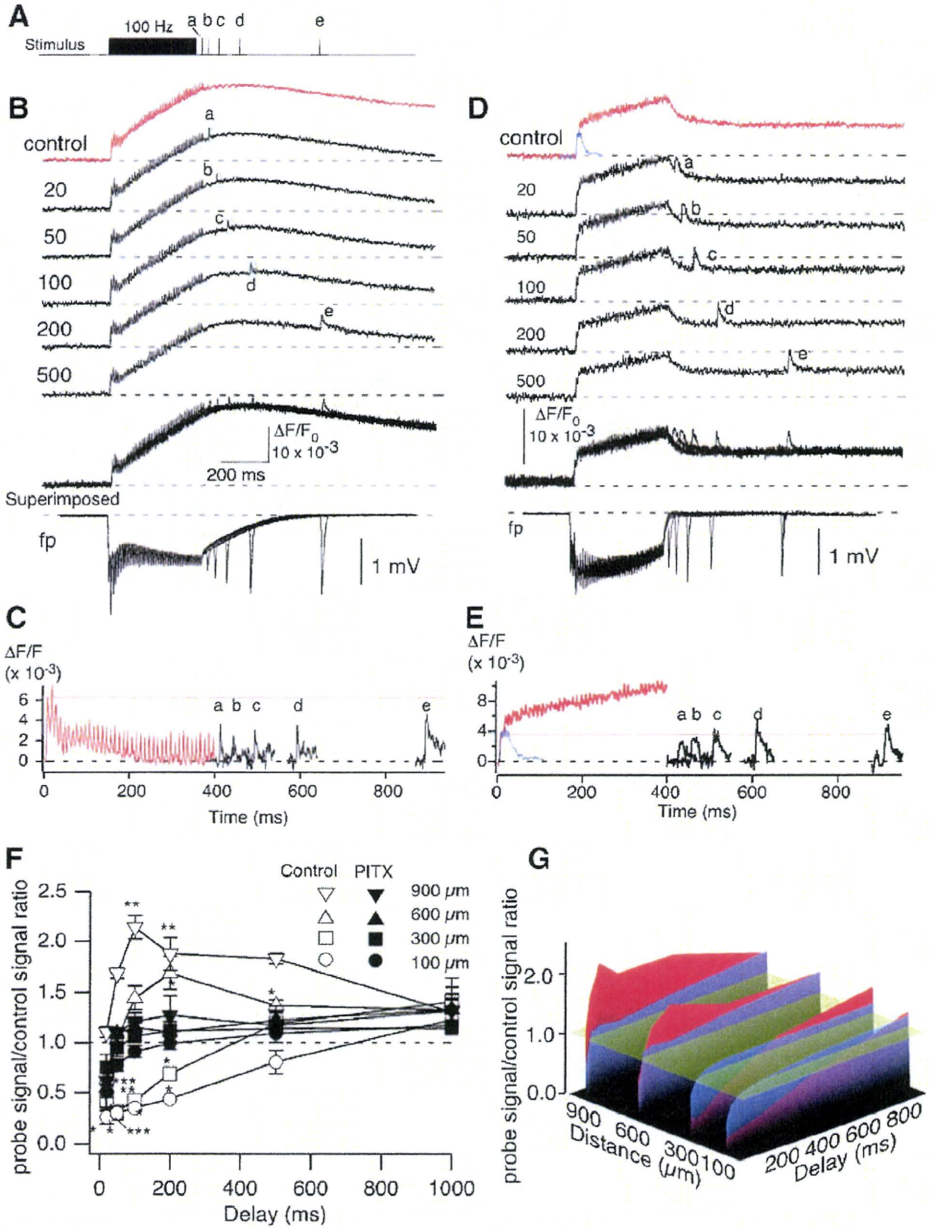

Fig. 4 Recovery of EPSP amplitude after incremental inhibition in normal aCSF (**b**, **c**) and in the presence of the GABA$_A$ receptor antagonist PiTX (**d**, **e**). **a** Schematic drawing of stimulus timing. Delayed single stimuli used to probe EPSP amplitude after cessation of tetanic stimulation (20, 50, 100, 200, and 500 ms posttetanus delay) are shown in the same trace (**a**–**e**). **b** Representative trace of the optical signal recorded in response to tetanic stimulation (100 Hz, 40 pulses; *red line*; control) and variable-interval probe traces (**a**–**e**) obtained at the same pixel in response to a single stimulus. *Bottom trace* shows superimposed control and all probe traces of the optical signal and the corresponding field potential (*fp*) recorded in the middle of stratum radiatum. **c** Comparison of EPSP amplitudes in optical recordings after the long-depolarizing component was removed using the same subtraction method presented in Fig. 1. *Red trace* shows the resulting individual trace obtained during the tetanus, and the subsequent *black traces* show the resulting probe EPSPs traces, **a**–**e**, all as a function of time from the start of the high-frequency stimulation. The probe responses were obtained by subtracting the control response (red trace in **b**) from the responses to probing episodes. Probe traces and traces recorded during the tetanus are drawn on same time scale. **d** The same responses as shown in **b** in the presence of PiTX. **e** Time course of the optical signal during tetanic stimulation in the presence of PiTX (*blue trace*) and the subtracted responses to delayed probe stimuli; same time scale. *Thin red horizontal line* shows the amplitude of the initial EPSP. **f** Pooled data of the amplitude of the probe signals relative to the control signal at points 100, 300, 600, and 900 µm away from the stimulation site in control solution (*open symbols*) and in the presence of PiTX (*filled symbols*). Time scale shows the delay from the cessation of tetanus. ***P<0.001; **P<0.01; *P<0.5, one-way ANOVA with Tukey's test. n=6. *Error bars*, SEM. **g** Three-dimensional presentation of pooled data shown in **f**. The *red colored plots* show interpolated mean values of time course shown in the control solution. The *blue colored plots* show the time course in the presence of PiTX

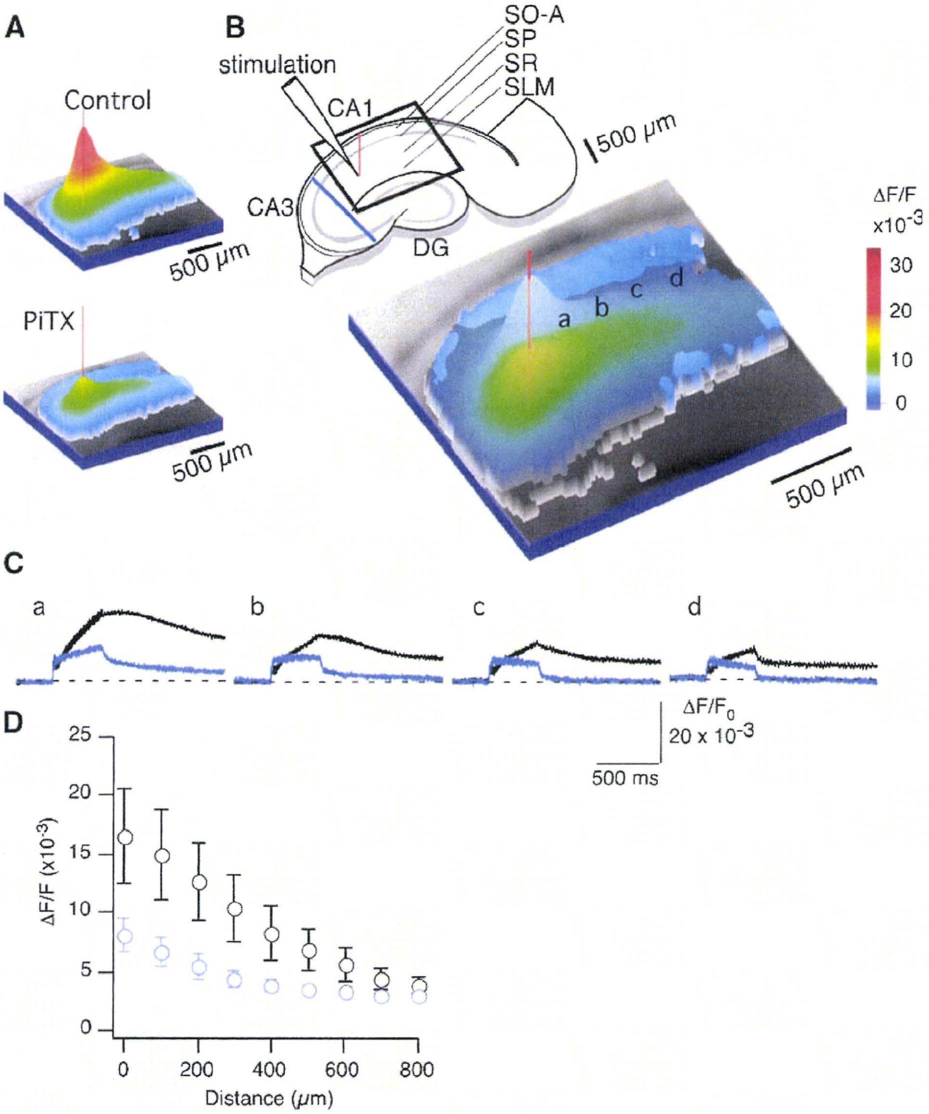

Fig. 5 Inhibition of GABA$_A$ receptors reduces distance-dependent long-lasting depolarization. **a** Three-dimensional plots showing the maximum amplitudes of CA1 neuronal responses to tetanic stimulation (100 Hz, 40 pulses) in slices bathed in normal aCSF (control) and in aCSF containing 100 μM PiTX. Amplitudes are mapped according to each corresponding pixel. *Red vertical lines* represent the stimulation site in the slice. **b** Superimposed three-dimensional plots for the control (*grayscale*) and PiTX (*pseudocolored*) conditions. A reference three-dimensional illustration represents the hippocampus, the stimulation electrode, and the field of view of the imaging system (*square*). *SO-A* stratum oriens–alveus, *SP* stratum pyramidale, *SR* stratum radiatum, *SL-M* stratum lacunosum–moleculare. **c** Representative traces of the optical signal obtained from single pixels at various locations in stratum radiatum (*a–d* correspond to locations shown in **b**). *Black traces* show control responses, and *blue traces* show responses in the presence of PiTX. **d** Response peak amplitudes at the tail end of the responses, which were sampled 200 ms after the end of tetanic stimulation (*n*=4, control; *n*=4, PiTX). *Error bars* are SEM (see also Supplemental movie s3.mpg.)

effectively removed by application of PiTX, which is especially evident in distal parts of CA1 distal (toward the subiculum).

Summarized data are shown in Fig. 5d, in which the response amplitude measured at 200 ms from cessation of tetanic stimulation is plotted as a function of distance from the site of stimulation. Here, the averages of the tetanus-induced responses clearly demonstrate the effect of antagonizing CA1 GABA$_A$ receptors: The distribution of the response across a wide transverse area of the proximal part of the apical dendritic field of CA1 was attenuated and more uniformly excitatory. We conclude that the application of a GABA$_A$ receptor antagonist makes the distribution of the tetanus-induced response more uniform or flattens it (for an animated presentation of these findings, see Supplemental movie s5.mpg).

Enhanced propagation following tetanus-induced incremental inhibition of EPSPs

Next, we examined the effect of distance on the recovery of EPSP amplitude from incremental inhibition (Fig. 6) after tetanic stimulation. The traces in Fig. 6a show time- and distance-ordered traces of the optical signal in response to tetanic stimulation and to delayed probe stimuli delivered at various delays after the end of the tetanus (increasing delays, ordered top to bottom; increasing distance from stimulation site, ordered left to right). The probe responses were obtained by subtracting the control response (the response to high-frequency stimulation only, i.e., traces presented at 0 ms in a–d of Fig. 6a) from the responses to the probing episodes (traces presented at 20, 50, 100, 200, and 500 ms in a–d of Fig. 6a). Representative traces of the

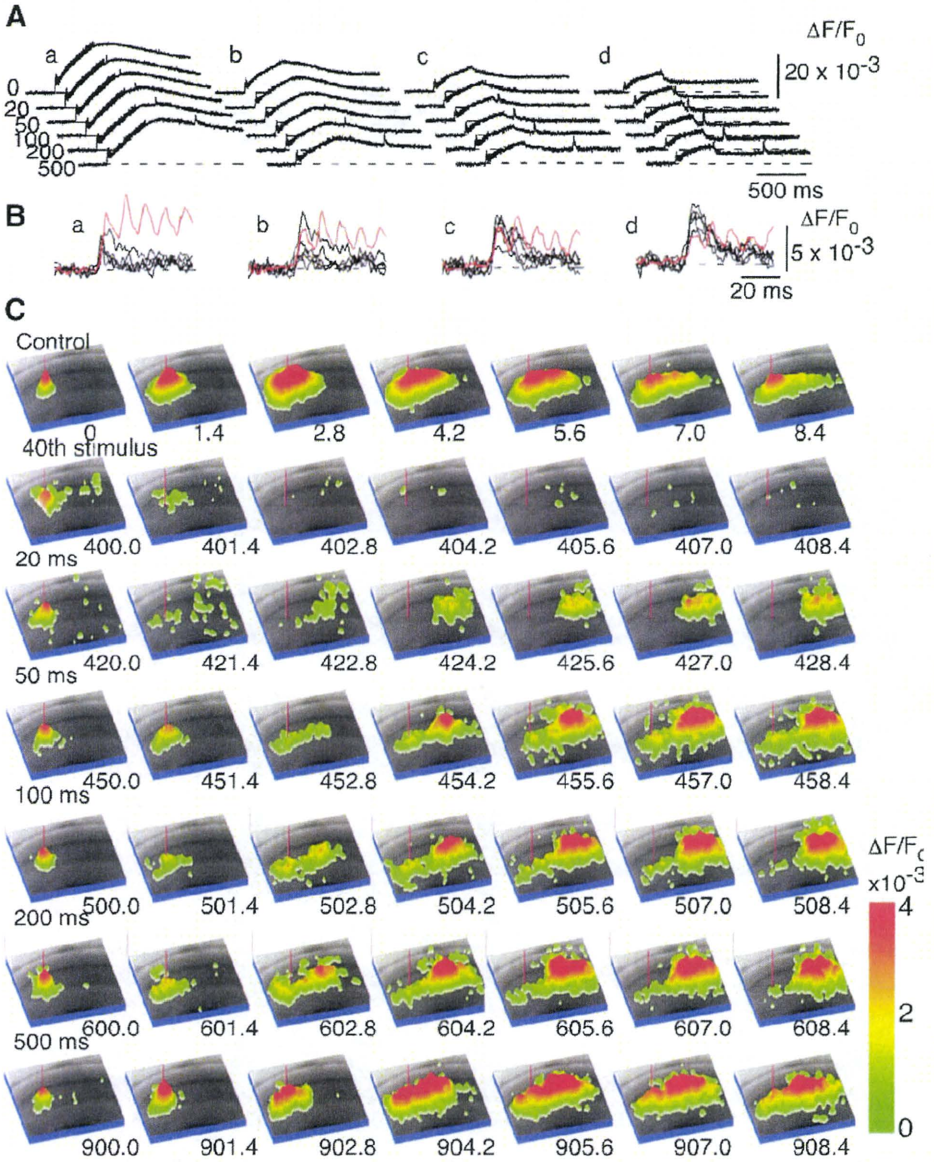

Fig. 6 Distance-dependent inhibition and enhancement of EPSPs in CA1 of rat hippocampal slices after tetanic stimulation. **a** Representative traces of the optically detected neuronal responses elicited by tetanic stimulation (100 Hz, 40 pulses) and following single stimulation with various delays (20, 50, 100, 200, and 500 ms; 0 is no delay) from the end of the tetanic stimulation at various distances from the site of stimulation (*a* 200 μm, *b* 400 μm, *c* 600 μm, and *d* 800 μm). Probe responses are visible as smaller, delayed, sharp depolarizations riding on the tail of the response. **b** Traces represent the probe responses after subtraction, which are displayed on expanded time and amplitude scales and aligned to the start of high-frequency stimulation. The *red traces* superimposed on the subtracted traces represent the initial phase of the response to tetanus. **c** Consecutive three-dimensional plots show pseudocolored activity maps of the neural response as it appears in the optical signal. *Red vertical lines* represent stimulating electrode. The *topmost row* (control) shows the pattern of neuronal excitation propagation of the response to the first stimulus of the tetanic stimulation, displayed every 1.4 ms. The *second row* (40th pulse) shows the pattern of propagation with the last (40th pulse) stimulus, after subtraction of the long-lasting component. The *subsequent rows* show the propagation pattern of neuronal excitation to the delayed probe stimulus after the subtraction of the response by the control response at delays of 20, 40, 100, 200, and 500 ms, respectively (see also Supplemental movie s4.mpg.)

subtracted signals are superimposed and shown in a–d of Fig. 6b (a of Fig. 6a is the same trace shown in Fig. 4b.)

At a pixel near the stimulation site, the peak amplitudes of the responses to single probe stimuli delivered after cessation of the tetanus were smaller than the responses to the first stimulus of the tetanic stimulation. These gradually recovered with increasingly long intervals, as before (a of Fig. 6a). On the other hand, at a pixel far from the stimulating site and at

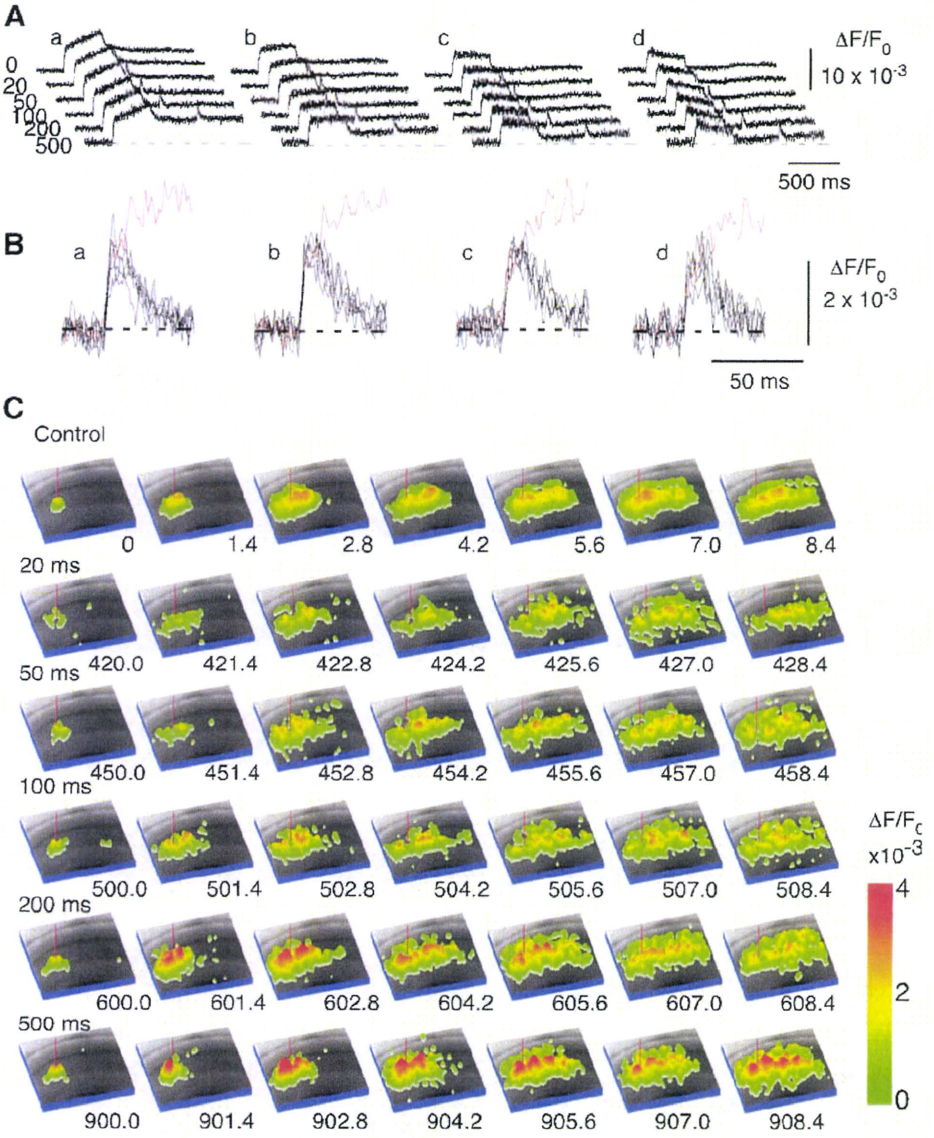

Fig. 7 Antagonism of $GABA_A$ receptors "homogenizes" probe responses in spatial and time domains following tetanic stimulation. Experiments were conducted with 100 μM PiTX in the slice chamber perfusate. The same high-frequency stimulation and delayed single probe stimulus protocol and subtraction procedure were used as in earlier experiments. **a** Representative traces of the optical signal recorded in stratum radiatum following the tetanus and the delayed posttetanus probe responses to single stimuli delivered at 20, 50, 100, 200, and 500 ms (*ordered top to bottom*, respectively) after the tetanus. Probe responses are visible as smaller, delayed, sharp depolarizations riding on the tail of the response. **b** *Traces ordered left to right* were obtained from individual pixels located at increasing distances from the site of stimulation (*a* 200 μm, *b* 400 μm, *c* 600 μm, and *d* 800 μm). *Lower traces* represent the probe responses after subtraction. These are displayed on expanded time and amplitude scales and aligned to the start of high-frequency stimulation. The *red traces* superimposed on the subtracted traces represent the initial phase of the response to tetanus stimulation in the presence of PiTX. **c** Consecutive images of the optical signal amplitude showing the propagation of neuronal excitation in response to the first stimulus of the tetanus (*first row*; control) and those to the delayed probe stimuli. The *red vertical lines on the images* show the site of stimulation (1.4 ms/images; see also Supplemental movie s5.mpg)

short intervals, the probe response was slightly larger than its control and became even larger as the posttetanus probe intervals increased (d of Fig. 6b). As b and c of Fig. 6b illustrate, we observed an intermediate-sized effect at distances and intervals between these extremes.

Figure 6c shows the propagation pattern in terms of a time-lapsed three-dimensional image of the optical signal. The propagation of the response to the last stimulus (40th pulse) of the tetanus (second row, Fig. 6c) was far smaller than that to the first stimulus (first row, control). The response for the latter case was confined almost entirely to the area immediately around the stimulating site. Twenty milliseconds after tetanus cessation, the propagation recovered a small amount from the inhibition (third row, Fig. 6c), especially at distal parts of CA1, far from the stimulating site. As the delay between tetanus cessation and probe stimulus increased, the distance-dependent recovery of the propagation got clearer. Moreover, the response clearly was enhanced distally with progressively more delayed probe stimuli. In other words, we observed time-dependent enhancement of neuronal activity propagation after high-frequency stimulation ended (for an animated presentation of these findings, see Supplemental movie s4.mpg).

The effect of PiTX on the distance-dependent recovery and enhancement of the response is shown in Fig. 7; the same delayed, single probe stimulus and subtraction protocol was used as in earlier experiments. As is clear in the subtracted traces of the probe responses (Fig. 7b), the response amplitudes did not change much, irrespective of the length of the delay or the distance from the stimulating site.

When comparing the three-dimensional plots of Fig. 6c (no PiTX) to those of Fig. 7c, it becomes especially clear that the pattern of response propagation in the presence of PiTX varies little between the control case (only tetanus, no probe stimuli) and the experimental case (tetanus plus probe stimuli). That is, the application of PiTX diminished the asymmetry of the typical tetanus-induced response in the space and time domains, approaching an overall uniformity of depolarization over a large area of the transverse plane of CA1.

Discussion

Membrane potential responses to tetanic burst stimulation (100 Hz, 40 pulses) of Schaffer collateral afferents in CA1 of rat hippocampal slice preparations were examined by means of optical recording of membrane potentials as well as by conventional patch-clamp and field potential recordings. We demonstrated that burst stimulation caused a long-lasting depolarization observable in the optical signal near the stimulating site, which was accompanied by a progressive decrease in EPSP amplitude. In contrast, the long-lasting depolarization was weaker when the distance from the stimulation site was increased. However, after cessation of the tetanic stimulation, we observed subsequent facilitation of individual EPSPs for up to 1,000 ms in sites further than 600 μm. The long-lasting depolarization and the progressive decrease and facilitation of EPSPs were diminished by application of PiTX and were thus dependant on $GABA_A$ receptors. Taking the voltage-clamp experiments (Fig. 3) into account, we hypothesize that this intense stimulation causes spill over of GABA, which in turn induces long-lasting depolarization at the postsynaptic membrane. On studying a wider portion of CA1 using the optical-imaging method, we observed that the same stimulus facilitated excitation propagation and that this effect was dependent on $GABA_A$ receptors. A recent study showed enhanced activation of $GABA_A$ receptors after an acute perfusion of di-4-ANEPPS to cultured neurons [41]; however, we did not observe any qualitative difference in the physiology of slice preparations after the wash.

Synaptically released GABA causes long-lasting depolarization at the postsynaptic membrane

Blockage of the long-lasting depolarization by the $GABA_A$ receptor antagonist PiTX (Figs. 3, 4, and 5) is consistent with lines of evidence showing that high-frequency stimulation can induce sustained $GABA_A$ receptor-dependent depolarization under certain conditions [19, 27, 44, 51, 53]. The reversal of the long-lasting membrane current (Fig. 3a) corroborates this. This kind of depolarization is mostly caused by a depolarizing $GABA_A$ receptor response [1, 52] related to excess GABA accumulation.

It is widely accepted that the depolarizing $GABA_A$ receptor potential is mediated by a shift in the reversal potential of the $GABA_A$ receptor channel (E_{GABA}), from hyperpolarizing to depolarizing, while the possible involvement of different types of extrasynaptic $GABA_A$ receptor channels [2] is still suspected. It is also accepted that the shift of E_{GABA} involves processes that mostly depend on a change in the intracellular Cl^- concentration caused by the changes in the extracellular ionic environment (mostly HCO_3^-, K^+, Cl^- ions) mediated by the high-frequency stimulation [27, 32, 34, 51, 53]; also see the recent reviews by [23, 43, 52].

Synaptically released GABA causes modulation of excitatory transmission

We have shown that a progressive decrease of EPSPs occurs in an area where the long-lasting depolarization wasprominent (Figs. 1 and 2). We postulate that this area accumulates excess GABA (Fig. 5). Excess GABA may inhibit EPSPs directly through typical $GABA_A$ receptor actions at the postsynaptic cell, for example, shunting of excitatory current. However, we demonstrated incremental inhibition of EPSCs under voltage-clamp conditions (Fig. 3). The usual direct postsynaptic $GABA_A$ receptor actions cannot reduce EPSCs as we describe here. The reduced EPSCs may be attributable to disruption of space-clamp condition due to massively reduced input conductance by $GABA_A$ receptors. However, it is not clear that to what extent this can affect to the amplitude of the EPSCs. A complete reversal of the long-lasting current on the depolarized holding potential may indicate that the membrane potential is still under the control of the voltage-clamp condition, at least at the site where the $GABA_A$ receptors are functional; thus, disruption of the space-clamp condition would not have a considerable effect on the amplitude of the EPSCs. In addition, the time course of the EPSC, which should be altered under a disrupted space-clamp condition, did not change to a great extent, even at the end of the train of stimulation. This may reduce the feasibility of the effect of disruption of the space-clamp condition on EPSCs. It is also not feasible to postulate unknown postsynaptic crosstalk between $GABA_A$ receptor activation and glutamate receptors because even at a depolarizing holding potential, we observed the progressive decrease of EPSCs. In addition, because $GABA_A$ receptor antagonists diminish the progressive decrease, presynaptic neurotransmitter depletion cannot account for the progressive decrease.

Alternatively, we postulate that direct $GABA_A$ receptor-mediated inhibition of excitatory synaptic transmission accounts for the progressive decrease of EPSPs. Presynaptic $GABA_A$ receptor-mediated modulation of synaptic transmission has been observed in many areas of the CNS, following its first description in the spinal cord [21, 22]. It has also been found to occur at mossy fiber synapses in hippocampal CA3 [30, 31, 45].

Activation of presynaptic $GABA_A$ receptors can modulate glutamate release in downward [45] and upward [30] directions. Hence, it is reasonable to propose that the activation of presynaptic $GABA_A$ receptors is the cause of the incremental inhibition and also the subsequent facilitation of propagation of excitation shown in this study. The other possible explanation could be conduction block of axons caused by axonal $GABA_A$ receptors [59]. It is interesting to point out that in Fig. 1d, the presynaptic fiber activity seemed to be decreased somewhat compared to that recorded in low Ca^{2+} solution. The mechanism underlying this finding may involve elevation of extracellular K^+ levels [34] by sustained depolarization of postsynaptic neurons, which in turn induces conduction blockage of the presynaptic axonal fibers [55]. However, it remains unclear whether this hypothesis accounts for the dramatic decrease in postsynaptic response (Fig. 1b).

Plausible mechanisms of the late "super recovery" or response facilitation

Response enhancement following high-frequency stimulation may be posttraumatic hyperexcitability [46], tetanic stimulation-induced gamma- and beta-band oscillations [10, 58, 62] and seizure-like activity [25, 29], and/or posttetanic potentiation. The mechanisms of these augmented kinds of excitability induced by high-frequency stimulation remain unclear, as far as we know. However, it is interesting to note that the enhancement after the tetanus in the present experiment was more prominent at progressively more distal sites in the transverse axis of CA1 (i.e., toward the subiculum), regions where the long-lasting depolarization was not prominent and/or the incremental inhibition was prominent. The response at a distance of 300 μm from the site of tetanus application showed enhancement only after 20 ms or more elapsed since the end of the tetanus, while inhibition was still prominent at more proximal sites (toward the stimulating electrode at the CA3–CA1 border). The late "super recovery" of EPSPs at distant sites from the stimulation electrode as well as the transient decrease of EPSPs at proximal sites was sensitive to PiTX. Thus, the opposite short-term modulations of excitatory transmission were both dependent on activation of $GABA_A$ receptors. We propose a balance between inhibitory and facilitative action of excess GABA accumulation: At higher concentrations, excess GABA accumulation may inhibit neural signal transduction, whereas at lower concentrations, it may facilitate neural signal transduction, possibly by different mechanisms. Transient weakening of inhibition due to transient reversal of membrane potential response [8] may account for the late "super recovery". The same electrical stimulation can recruit a short-term GABAergic spatially differentiated modulation in neural circuits when it was encoded into a 100-Hz tetanic stimulation. This may highlight the GABAergic action in frequency-dependent neuronal signal processing.

Physiological implication of the tetanus-induced response changes in space and time

The tetanic stimulation used in the present study is one of the most common stimulation protocols used to induce LTP, and indeed, it mimics hippocampal pyramidal cell bursting observed during learning behavior [64]. The incremental inhibition of excitation propagation we observed during tetanic afferent stimulation is important for understanding more clearly the neural basis of information processing that presumably is embedded in neuronal bursting [12, 14, 28, 63]. The powerful influence of the GABA circuitry in shaping the patterns of CA1 excitatory activity in response to tetanic stimulation in space and time domains demonstrated here suggests that external influences on this GABA circuitry will have a profound impact on bursting-mediated information flow through the hippocampus. $GABA_A$ receptor-dependent inhibition would also be an important stabilizing factor for $GABA_A$ receptor-dependent synchronized activity mediated by the interneuron network of hippocampus [49].

The steep spatial convergence of GABA$_A$ receptor-dependent heterogenic progressive decrease and facilitation of EPSP (Figs. 4, 5, 6 and 7) would also be important to shaping heterogenic LTP induction [16, 56]. The subsequent enhancement of EPSP at distal portion can also account for the heterogenic induction of LTP.

To our knowledge, little is known about the presynaptic GABA$_A$ receptor-mediated modulation of glutamatergic synaptic transmission in the Schaffer collateral pathway of area CA1. If the present incremental inhibition does indeed occur in behaving animals, then it would represent a new aspect of GABA-mediated modulation of information flow through and beyond area CA1 of the hippocampus.

Acknowledgments We thank Dr. Michinori Ichikawa for his kind encouragement and help during the early phase of this work and Dr. Michael E. Barish for his critical comments on an earlier version of the manuscript.

References

1. Alger BE, Nicoll RA (1979) GABA-mediated biphasic inhibitory responses in hippocampus. Nature 281:315–317
2. Alger BE, Nicoll RA (1982) Pharmacological evidence for two kinds of GABA receptor on rat hippocampal pyramidal cells studied in vitro. J Physiol (Lond) 328:125–141
3. Ang CW, Carlson GC, Coulter DA (2006) Massive and specific dysregulation of direct cortical input to the hippocampus in temporal lobe epilepsy. J Neurosci 26:11850–11856
4. Bai L, Huang X, Yang Q, Wu JY (2006) Spatiotemporal patterns of an evoked network oscillation in neocortical slices: coupled local oscillators. J Neurophysiol 96:2528–2538
5. Bartos M, Vida I, Jonas P (2007) Synaptic mechanisms of synchronized gamma oscillations in inhibitory interneuron networks. Nat Rev Neurosci 8:45–56
6. Beau FENL, Alger BE (1998) Transient suppression of GABAA-receptor-mediated IPSPs after epileptiform burst discharges in CA1 pyramidal cells. J Neurophysiol 79:659–669
7. Ben-Ari Y, Gaiarsa JL, Tyzio R, Khazipov R (2007) GABA: a pioneer transmitter that excites immature neurons and generates primitive oscillations. Physiol Rev 87:1215–1284
8. Blaesse P, Airaksinen MS, Rivera C, Kaila K (2009) Cation-chloride cotransporters and neuronal function. Neuron 61:820–838
9. Bliss TVP, Collingridge GL (1993) A synaptic model of memory: long-term potentiation in the hippocampus. Nature 361:31–39
10. Bracci E, Vreugdenhil M, Hack SP, Jefferys JG (1999) On the synchronizing mechanisms of tetanically induced hippocampal oscillations. J Neurosci 19:8104–8113
11. Broicher T, Bidmon H-J, Kamuf B, Coulon P, Gorji A, Pape H-C, Speckmann E-J, Budde T (2010) Thalamic afferent activation of supragranular layers in auditory cortex in vitro: a voltage sensitive dye study. Neuroscience 165:371–385
12. Buzsaki G, Horvath Z, Urioste R, Hetke J, Wise K (1992) High-frequency network oscillation in the hippocampus. Science 256:1025–1027
13. Buzsaki G, Leung LW, Vanderwolf CH (1983) Cellular bases of hippocampal EEG in the behaving rat. Brain Res 287:139–171
14. Buzsaki G, Penttonen M, Nadasdy Z, Bragin A (1996) Pattern and inhibition-dependent invasion of pyramidal cell dendrites by fast spikes in the hippocampus in vivo. Proc Natl Acad Sci USA 93:9921–9925
15. Carriero G, Uva L, Gnatkovsky V, de Curtis M (2009) Distribution of the olfactory fiber input into the olfactory tubercle of the in vitro isolated guinea pig brain. J Neurophysiol 101:1613–1619
16. Chang PY, Jackson MB (2006) Heterogeneous spatial patterns of long-term potentiation in rat hippocampal slices. J Physiol 576:427–443
17. Cohen LB, Salzberg BM (1978) Optical measurement of membrane potential. Rev Physiol Biochem Pharmacol 83:35–88
18. Coulter DA, Carlson GC (2007) Functional regulation of the dentate gyrus by GABA-mediated inhibition. Prog Brain Res 163:235–243
19. Davies CH, Collingridge GL (1993) The physiological regulation of synaptic inhibition by GABAB autoreceptors in rat hippocampus. J Physiol 472:245–265
20. de Curtis M, Takashima I, Iijima T (1999) Optical recording of cortical activity after in vitro perfusion of cerebral arteries with a voltage-sensitive dye. Brain Res 837:314–319
21. Dudel J, Kuffler SW (1961) Presynaptic inhibition at the crayfish neuromuscular junction. J Physiol 155:543–562
22. Eccles JC, Schmidt R, Willis WD (1963) Pharmacological studies on presynaptic inhibition. J Physiol 168:500–530
23. Farrant M, Kaila K (2007) The cellular, molecular and ionic basis of GABA(A) receptor signalling. Prog Brain Res 160:59–87
24. Fries P, Nikolic D, Singer W (2007) The gamma cycle. Trends Neurosci 30:309–316
25. Fujiwara-Tsukamoto Y, Isomura Y, Imanishi M, Fukai T, Takada M (2007) Distinct types of ionic modulation of GABA actions in pyramidal cells and interneurons during electrical induction of hippocampal seizure-like network activity. Eur J Neurosci 25:2713–2725
26. Grinvald A, Hildesheim R (2004) VSDI: a new era in functional imaging of cortical dynamics. Nat Rev Neurosci 5:874–885
27. Grover LM, Lambert NA, Schwartzkroin PA, Teyler TJ (1993) Role of HCO3− ions in depolarizing GABAA receptor-mediated responses in pyramidal cells of rat hippocampus. J Neurophysiol 69:1541–1555
28. Harris KD, Hirase H, Leinekugel X, Henze DA, Buzsaki G (2001) Temporal interaction between single spikes and complex spike bursts in hippocampal pyramidal cells. Neuron 32:141–149
29. Isomura Y, Fujiwara-Tsukamoto Y, Takada M (2003) Glutamatergic propagation of GABAergic seizure-like after discharge in the hippocampus in vitro. J Neurophysiol 90:2746–2751
30. Jang IS, Ito Y, Akaike N (2005) Feed-forward facilitation of glutamate release by presynaptic GABA(A) receptors. NeuroReport 135:737–748
31. Jang IS, Nakamura M, Ito Y, Akaike N (2006) Presynaptic GABAA receptors facilitate spontaneous glutamate release from presynaptic terminals on mechanically dissociated rat CA3 pyramidal neurons. NeuroReport 138:25–35
32. Kaila K, Lamsa K, Smirnov S, Taira T, Voipio J (1997) Long-lasting GABA-mediated depolarization evoked by high-frequency stimulation in pyramidal neurons of rat hippocampal slice is attributable to a network-driven, bicarbonate-dependent K+ transient. J Neurosci 17:7662–7672
33. Kaila K, Voipio J (1987) Postsynaptic fall in intracellular pH induced by GABA-activated bicarbonate conductance. Nature 330:163–165
34. Kaila K, Voipio J, Paalasmaa P, Pasternack M, Deisz RA (1993) The role of bicarbonate in GABAA receptor-mediated IPSPs of rat neocortical neurones. J Physiol 464:273–289
35. Kajiwara R, Takashima I, Mimura Y, Witter MP, Iijima T (2003) Amygdala input promotes spread of excitatory neural activity from perirhinal cortex to the entorhinal–hippocampal circuit. J Neurophysiol 89:2176–2184

36. Kajiwara R, Tominaga T, Takashima I (2007) Olfactory information converges in the amygdaloid cortex via the piriform and entorhinal cortices: observations in the guinea pig isolated whole-brain preparation. Eur J Neurosci 25:3648–3658
37. Kiritoshi T, Ikeda H, Murase K (2010) Long-term potentiation of neuronal excitation in the central nucleus of the rat amygdala revealed by imaging with a voltage-sensitive dye. Brain Res 1349C:32–34
38. Koganezawa N, Taguchi A, Tominaga T, Ohara S, Tsutsui K, Witter MP, Iijima T (2008) Significance of the deep layers of entorhinal cortex for transfer of both perirhinal and amygdala inputs to the hippocampus. Neurosci Res 61:172–181
39. Mann EO, Suckling JM, Hajos N, Greenfield SA, Paulsen O (2005) Perisomatic feedback inhibition underlies cholinergically induced fast network oscillations in the rat hippocampus in vitro. Neuron 45:105–117
40. Mann EO, Tominaga T, Ichikawa M, Greenfield SA (2005) Cholinergic modulation of the spatiotemporal pattern of hippocampal activity in vitro. Neuropharmacology 48:118–133
41. Mennerick S, Chisari M, Shu HJ, Taylor A, Vasek M, Eisenman LN, Zorumski CF (2010) Diverse voltage-sensitive dyes modulate GABAA receptor function. J Neurosci 30:2871–2879
42. Paulsen O, Sejnowski TJ (2006) From invertebrate olfaction to human cognition: emerging computational functions of synchronized oscillatory activity. J Neurosci 26:1661–1662
43. Payne JA, Rivera C, Voipio J, Kaila K (2003) Cation-chloride co-transporters in neuronal communication, development and trauma. Trends Neurosci 26:199–206
44. Perreault P, Avoli M (1989) Effects of low concentrations of 4-aminopyridine on CA1 pyramidal cells of the hippocampus. J Neurophysiol 61:953–970
45. Ruiz A, Fabian-Fine R, Scott R, Walker MC, Rusakov DA, Kullmann DM (2003) GABAA receptors at hippocampal mossy fibers. Neuron 39:961–973
46. Santhakumar V, Voipio J, Kaila K, Soltesz I (2003) Post-traumatic hyperexcitability is not caused by impaired buffering of extracellular potassium. J Neurosci 23:5865–5876
47. Sejnowski TJ, Paulsen O (2006) Network oscillations: emerging computational principles. J Neurosci 26:1673–1676
48. Sinha SR, Saggau P (1999) Optical recording from populations of neurons in brain slices. In: Windhorst U, Johansson H (eds) Modern techniques in neuroscience research. Springer, Berlin, p 459486
49. Sinha SR, Saggau P (2001) Imaging of 4-AP-induced, GABAA-dependent spontaneous synchronized activity mediated by the hippocampal interneuron network. J Neurophysiol 86:381–391
50. Staley KJ, Proctor WR (1999) Modulation of mammalian dendritic GABA(A) receptor function by the kinetics of Cl− and HCO3− transport. J Physiol Lond 519:693–712
51. Staley KJ, Soldo BL, Proctor WR (1995) Ionic mechanisms of neuronal excitation by inhibitory GABAA receptors. Science 269:977–981
52. Stein V, Nicoll RA (2003) GABA generates excitement. Neuron 37:375–378
53. Taira T, Lamsa K, Kaila K (1997) Posttetanic excitation mediated by GABA(A) receptors in rat CA1 pyramidal neurons. J Neurophysiol 77:2213–2218
54. Tominaga T, Tominaga Y, Ichikawa M (2001) Simultaneous multi-site recordings of neural activity with an inline multi-electrode array and optical measurement in rat hippocampal slices. Pflügers Arch Eur J Physiol 443:317–322
55. Tominaga T, Tominaga Y, Ichikawa M (2002) Optical imaging of long-lasting depolarization on burst stimulation in area CA1 of rat hippocampal slices. J Neurophysiol 88:1523–1532
56. Tominaga T, Tominaga Y, Yamada H, Matsumoto G, Ichikawa M (2000) Quantification of optical signals with electrophysiological signals in neural activities of Di-4-ANEPPS stained rat hippocampal slices. J Neurosci Methods 102:11–23
57. Tominaga Y, Ichikawa M, Tominaga T (2009) Membrane potential response profiles of CA1 pyramidal cells probed with voltage-sensitive dye optical imaging in rat hippocampal slices reveal the impact of GABA(A)-mediated feed-forward inhibition in signal propagation. Neurosci Res 64:152–161
58. Traub RD, Whittington MA, Stanford IM, Jefferys JGR (1996) A mechanism for generation of long-range synchronous fast oscillations in the cortex. Nature 383:621–624
59. Trigo FF, Marty A, Stell BM (2008) Axonal GABAA receptors. Eur J Neurosci 28:841–848
60. Tu B, Gu Z, Shen JX, Lamb PW, Yakel JL (2009) Characterization of a nicotine-sensitive neuronal population in rat entorhinal cortex. J Neurosci 29:10436–10448
61. Voipio J, Kaila K (2000) GABAergic excitation and K(+)-mediated volume transmission in the hippocampus. Prog Brain Res 125:329–338
62. Whittington MA, Stanford IM, Colling SB, Jefferys JGR, Traub RD (1997) Spatiotemporal patterns of gamma frequency oscillations tetanically induced in the rat hippocampal slice. J Physiol Lond 502:591–607
63. Wu JY, Guan L, Tsau Y (1999) Propagating activation during oscillations and evoked responses in neocortical slices. J Neurosci 19:5005–5015
64. Ylinen A, Bragin A, Nadasdy Z, Jando G, Szabo I, Sik A, Buzsaki G (1995) Sharp wave-associated high-frequency oscillation (200-Hz) in the intact hippocampus—network and intracellular mechanisms. J Neurosci 15:30–46

生物物理 51（2）, 092-095（2011）

理論／実験 技術

実践！ 膜電位感受性色素による神経回路解析

冨永貴志[1,2]，冨永洋子[1]
[1]徳島文理大学香川薬学部
[2]理化学研究所脳科学総合研究センター

1. はじめに

1966年の映画「ミクロの決死圏」では，小さくなって体の中を探検する科学者ら一行が，脳に到着して，神経細胞が軸索を走る光のパルスで情報のやり取りするさまを目の当たりにした．彼らが見たように，神経細胞同士が脳内で情報が伝えられるさまを眼で見られたら…．ヒトの脳が140億個もの神経細胞からできているのに，現在の最新のPC用CPU（インテルCore i7）でも，そのトランジスタ数がたった10億個程度であることを考えれば，これが脳の研究者の自然な欲求であることが理解できよう．この情報処理装置（CPU/脳）のはたらきを理解するためには1個1個の素子（トランジスタ／神経細胞）の動作のみならず，回路としての活動を目に見える形で知りたいのだ．ここでは，それを実現する手法の1つとして，膜電位感受性色素（Voltage Sensitive Dye; VSD）という特殊な色素分子による神経活動の可視化について解説する．今回は特に学部の実習のレベルでも実行可能な「容易な」技術となり得たことを紹介したい．

2. 光計測コトハジメ

神経細胞は，細胞膜内外の電位差（膜電位）の変化（神経興奮）という形で情報を伝えるので，その様は眼で見ることはできない．しかし，神経興奮に伴って複屈折性や光散乱などの光学的性質に微小な変化（10^{-5}-10^{-6}）が生じることは，1950年代から知られていた．膜電位変化をよりよく「見る」ために，ウッズホール海洋生物学研究所（MBL）の田崎一二らは蛍光共鳴エネルギー移動法（FRET）を用いて，この光学信号を増幅して計測した[1]．同研究所のLarry Cohenらのグループは，これをさらに発展させ，積極的に神経細胞の電気的信号を光学計測する色素の開発を行った[2]．これら1970年頃の研究が，現在の光計測の基礎となっている．

一般に細胞の膜電位は，ガラス微小電極のような電極を細胞膜へ刺して（あるいはくっつけて）細胞内の内液と電極内の電解質溶液を接触させ，そこから信号を取り出して増幅器で増幅して観測する．この電気生理学的手法の欠点は，電極の数を増やせないことであ

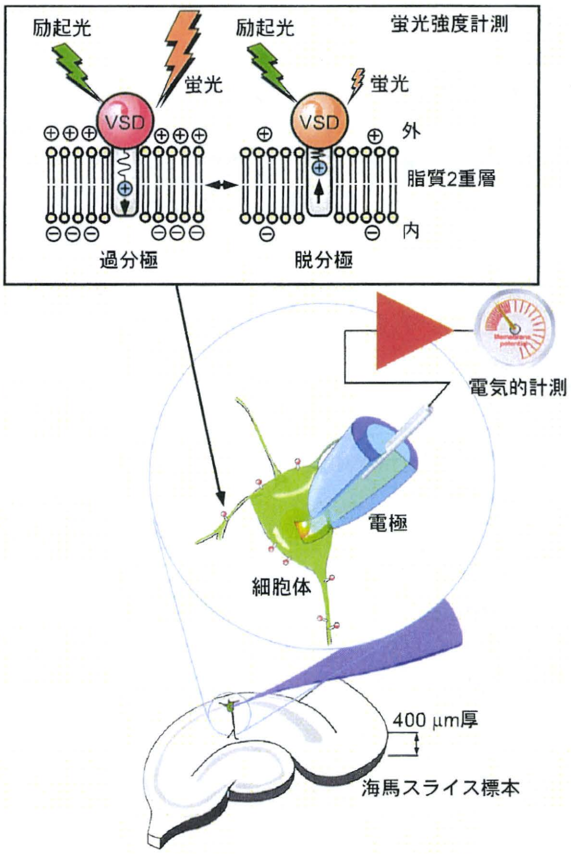

図1
脳海馬スライス標本における膜電位感受性色素（VSD）による計測（蛍光強度計測）と電極による計測（電気的計測）の模式図．VSDの蛍光は膜内の電界強度に依存して変化する．（電子ジャーナルではカラー）

Practices for the VSD Optical Recording Method of Neuronal Circuit Analysis

Takashi TOMINAGA[1,2] and Yoko TOMINAGA[1]
[1]Dept. Neurophysiol. Kagawa School of Pharmaceutical Sciences, Tokushima Bunri University
[2]Brain Science Institute, RIKEN

る．電極の大きさ，マニピュレータの配置などの制約のためである．一方，光計測では，細胞膜の脂質2重層に埋まって，膜を介した電界強度に応じた蛍光を生じる膜電位感受性色素の蛍光強度変化を計測する．そのため細胞や組織の各部位の電位変化を同時に計測することが可能である．

光計測には，高速・低雑音の特殊な撮像装置が必要である．日本では，東京医科歯科大学の神野耕太郎らのグループが独自の撮像装置を開発していた．また，電子技術総合研究所では松本元が，市川道教，飯島敏夫らを中心としたグループを率いて，市販化を念頭に精力的に撮像装置の開発を行った．このときに開発された浜松ホトニクス（株）製や，富士写真フィルム（株）製の撮像装置を，研究室にもっておられる方も多いのではないだろうか．海外では，Cohen や Grinvald ら研究者が早くから起業して光計測用撮像装置，色素を開発販売して普及させた．

一種の夢の技術が完成したと期待された当時の雰囲気を覚えていらっしゃる方も多いだろう3)-5)．膜電位感受性色素の一般の研究室での使用はその期待と高揚感の高さからいうと少し遅れて，21世紀に入ってから急速に使用され始めたようである6)．この後のセクションではこの遅れの原因となった技術的障壁のいくつかを解説したい．

3. 難しくしていたのはこれだ

3.1 光計測の困難さ―明るいのに暗い像

膜電位感受性色素の膜電位変化に対する応答は，よくて10^{-4}から10^{-3}程度（変化率）である．これは，カルシウム測光などで得られる信号サイズ（数十%から数百%）に比べるとたいへん小さい．また，神経細胞の活動に追随するためには，高速撮像が必須である．1ミリ秒から0.1ミリ秒の撮像速度（フレームレート）で計測できることが求められる．この精度（S/N値>60-70 dB）でこのフレームレートを実現する必要があるわけである．

変化率が小さいので，光の粒子性から生じる問題もある．n個の光粒子の数を数えるのに，$\sqrt{n}$個のエラーが確率的に生じる．光強度変化が10^{-3}程度のものだとしたら，$\sqrt{n}/n$が10^{-3}を超える必要があり，最低でも10^{6}個の光量子がいることになる．光計測に必要な撮像速度（だいたい1000フレーム毎秒）で，25 μm四方の撮像素子で計測するとして，1つの撮像素子で10^{6}の光量子数になる光（約10 μW/mm^{-2}）はかなり強い．結像面に薬包紙などをかざすと，特に暗室でなくとも像が裸眼で見える程度である．このように，他の蛍光測光などに携わっておられる方からすると感覚的には十分「明るい」画像も，光計測には「暗い」画像ということになる．

3.2 光源―安定で明るい光源がない

光計測ではなるべく「明るい」像を得ることが必要になるので明るい光源が求められる．顕微鏡光源でよく用いられるレーザー，高圧水銀灯，キセノンといった光源はミリ秒の世界では安定でない．レーザーでは数%のノイズとスペックルノイズ，高圧水銀灯，キセノンでは，火花（アーク）のゆらぎから生じるノイズが問題となる．そこで，（仕方なく）ハロゲン光源が一般的に用いられてきた．フィラメントの関係で150 W程度のハロゲン電球が最適といわれている．最近になって，ハイパワーのLEDが使用できるようになってきた．LEDは自己発熱に対する補正回路がついたものを選ぶ必要がある．

3.3 光学系―低倍で明るいものが必要だ

神経回路の機能解析のためには，神経回路そのものの大きさ（たとえば海馬の1領野や大脳皮質のカラム構造は500 μm四方程度）からいって総合倍率で1倍からせいぜい5倍までの光学倍率を選定する必要がある．この倍率で使える「明るい」落射蛍光顕微鏡がなかった．一般の生理の実験で使う正立顕微鏡で選べる対物レンズは（当時は）明るいものではなかった．倍率では，通常，実体顕微鏡が使われる領域になるが，適当なものがなくわれわれは独自の光学系を作成した．

3.4 機械的なノイズ―ほんのわずかな振動が

10^{-3}以下の安定性が必要なので，機械的なノイズも問題になる．振動で像が動く場合，像のもともとの光強度の不均一性に応じた大きなノイズ（～数十%）を拾う．ここで扱っている脳スライス標本からの光計測では，最も問題になるのは灌流液の水面の振動，スライス標本自体の動きである．

3.5 膜電位感受性色素の選択

膜電位感受性色素には大きく分けて，吸光度の変化を生じさせるものと，蛍光強度の変化を生じさせるものがある．吸光度の変化の場合，明るい像を得ることが比較的容易であるが，変化量を規格化することが困難である．蛍光色素は，光強度を規格化することで，比較的定量的な計測が可能となる．一方で，蛍光強度は比較的弱く光学系に工夫が必要である．

実験に使用する組織に応じて色素を選ぶ必要がある．スライス標本では，吸光色素のRH-155は水溶性が高く染色はしやすいが，洗い流されやすく長期間の計測には向かなかった．またグリア細胞の信号を強く検出する傾向がみられた．蛍光色素のRH-795も水溶

性が高く，長期の計測には不適であるが，*in vivo* の標本に適している．スライス標本では，溶けにくいが洗い流されにくいDi-4-ANEPPSが最適だった[7]．最近，ANNINE-6に注目しているがまだよい結果は得られていない．また，細胞内からの単一細胞染色にはDi-2-ANEPEQ（JPW114）を用いる．

4. 実際の応用例を少し

われわれは独自の光学系，後述するチャンバーシステム，ソフトウエアを開発して，定量的に光計測信号を扱えることを実証した[7]（図2）．これらを使ってトランスジェニック動物のアッセイや治療薬のシーズのアッセイを行うなどのことも可能になった[8]．また，テタヌス刺激がGABA(A)受容体を介した短期可塑性を引き起こすことなどを明らかにした[9]．また，活きた脳を取り出してその神経活動を計測することにも使われるようになってきた[10]．

5. 実習でも使える小型システムの開発

誰でも光計測を使って脳神経の活動を測れるようになれば，光計測のもつもともとの網羅性から，脳神経の病気やそれに対する薬をより早くアッセイできるに違いない．そこで，誰でも使えることを目標にシステムを構築した（図3）．

5.1 スライスチャンバー

脳スライス標本は，脳の神経回路機構を探るための非常に重要な標本である．しかし，この厚さ400 μmしかないフワフワして繊細なスライス標本の「活き」（生理学的な活性）を保ったまま取り扱うことはなかなか難しいことである．そこで，脳スライス標本を取り扱う器具に工夫を加え，スライス標本の取り扱いを容易にした[7]（図3上；特許3405301号，US 6448063）．この器具はスライス標本を保持する保持具と，実験時に生理的塩溶液を還流するための実験槽からなる．スライス標本の保持具は，アクリル樹脂のリングにミリポア社のメンブレンフィルター（OMNIPORE MEMBRANE FILTERS, 0.45 μm; JHWP01300）を貼りつけたものである．スライス標本はフィルターに張り付くので，このリングをもって操作できる．このフィルターは，ガスや生理塩溶液の良好な交換を可能とする．また，実験槽にはリングごと嵌め込むことで固定でき「重石」などがなくとも，スライス標本が動いてしまう心配はない．また，色素で染色する際，1枚あたり約100 μlの染色液で染色できるので高価な膜電位感受性色素を節約できる．さらに，この実験槽は目視のパッチクランプ実験にも用いることができ，筆者は400 μm厚のスライス標本でも斜光を使い良好に実験を行うことができている．

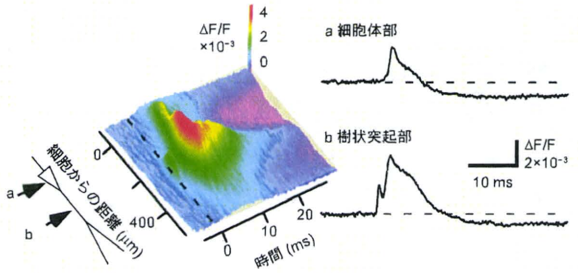

図2
海馬CA1野への電気刺激に対する膜電位応答を膜電位感受性色素によって計測したときの典型的な光信号［ΔF/F：初期蛍光強度（F）に対する蛍光強度の変化量（ΔF）比］．細胞に沿った電位変化分布の時間変化（左）と代表ピクセル（a：細胞体部，b：樹状突起部）での信号（右）．（電子ジャーナルではカラー）

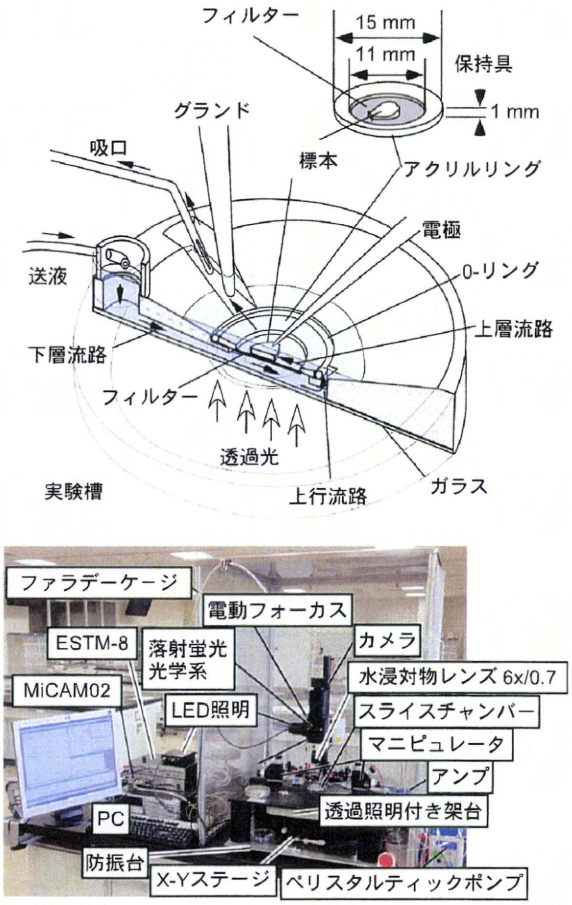

図3
チャンバーシステム図と実習システム写真．（電子ジャーナルではカラー）

5.2 光学系

光計測には，強い蛍光が必要である．先に述べたように適当な光学系がないことからわれわれは独自の光

学系を作製した．実体顕微鏡の対物レンズには開口数が大きなレンズがあったのでライカ社の実体顕微鏡用のレンズ（MZ-APO PLAN APO 1.0x）を投影レンズに使い，その間を無限遠焦点系とした落射蛍光光学系を作成した．実験槽中を還流している生理的塩溶液の水面がゆれると，機械的なノイズとして計測の邪魔になる．対物レンズとしては，オリンパス光学に依頼して開発した低倍の高開口数の水浸対物レンズ（MYCAM 10X/0.7, 5X/0.8）や，ブレインビジョン社の6X/0.7の水浸レンズなども使用できる．

5.3 光計測撮像装置と刺激装置

上記の光学系と，光学計測装置，マニピュレータ2台をセット可能な光学定盤を使って，最小システムを組み上げた（**図3**）．5 mm厚のステンレス板とソルボレインのダンパーで作成した防振台で十分な防振が得られる．これに，組み立て式のファラデーケージをかぶせて，暗幕で遮光している．光源は補正付きLEDを使用している．

光計測装置としてはブレインビジョン社のMiCAM-02を採用し，電気刺激装置としてESTM-8を採用した．電気生理学的な活性をモニターしつつ，光計測を行っている．

全体の大きさは，底面積で60 × 60 cm．高さが1 mである．これにPCが1台と電気生理用のアンプ（たとえばA-M Systems社，Model 3100）とペリスタルティックポンプがあれば実験が可能である．この大きさなら，通常の実験用机の一角でも複数台ならべて実験することができる．

5.4 ソフトウエア

実験の進行はIgorPro（Wavemetrics社）にマクロを組んで自動化している．このソフトウエアで随時電極から記録される神経応答（興奮性シナプス後電位，EPSP）を記録し，応答強度（初期EPSPスロープ）をリアルタイムでグラフにして表示している．このため，実験者は実験の結果をリアルタイムに見ることが可能である．このときの電気刺激と，電気応答の波形記録にはESTM-8を用いている．このソフトウエアは，要望があれば分けることができるので，必要な方は連絡してほしい．

6. おわりに

駆け足で，システムの紹介をしてきた．筆者は，このシステムで徳島文理大学薬学部の3年生を対象に学生実習を行っている．スライスは研究室で教員が作成する．午前中に10枚程度スライスを作成し，実習の開始時間に3階離れた実習室までスライスを運んで実験に供する．その後，電極の配置など目を配る必要はあるが，100名ほどの学生さんが脳スライス標本から解析に必要なレベルの光信号を計測している様は10年前には想像しにくかったことだ．光計測は，ふだんは見えない神経信号を目に見える形に変えてくれる．ディスプレーの上で動く膜電位変化の流れのようすを見るだけでも脳の信号処理の一端がイメージできる．これから長寿社会で神経関連の病気に社会をあげて対応する必要がある今，これを体験した人材を供給することは意義深い．

また，このシステムは小型で扱いやすく電気生理などの技術に熟練した計測者でなくとも複数の装置での同時データ取得が可能である．この利点を活かして，医薬品，食品成分，環境化学物質などの化学物質による神経影響評価への応用をめざした共同研究を，国立医薬品食品衛生研究所・毒性部の種村健太郎博士と進めている．

さて，ここまで簡単になって学部学生でもできるこの夢の実験系，使ってみてはいかがでしょうか？

この研究は平成18年，平成20，21年徳島文理大学「特色ある教育研究」ならびに厚生労働省科研費（H20-化学-一般-009）にサポートされた．

文 献

1） Tasaki, I. *et al.*（1968）Proc. Natl. Acad. Sci. USA **61**, 883.
2） Salzberg, B. M. *et al.*（1973）Nature **246**, 508.
3） 市川道教ら（1992）日本物理学会誌 **47**, 707-712.
4） 飯島敏夫ら（1994）生物物理 **34**, 219-222.
5） 松本　元（1995）生物物理 **35**, A25-A29.
6） Grinvald, A., Hildesheim, R.（2004）Nat. Rev. Neurosci. **5**, 874.
7） Tominaga, T. *et al.*（2000）J. Neurosci. Methods **102**, 11.
8） Tanemura, K. *et al.*（2002）J. Neurosci. **22**, 133.
9） Kajiwara, R. *et al.*（2007）Eur. J. Neurosci. **25**, 3648.
10） Tominaga, T., Tominaga, Y.（2010）Pflugers Arch. **460**, 875-889.


冨永貴志

冨永貴志（とみなが　たかし）
徳島文理大学香川薬学部准教授
理化学研究所脳科学総合研究センター客員研究員
理化学研究所脳科学総合研究センタースタッフサイエンティストなどを経て現職．
研究内容：光計測を使った脳機能解析，繊毛の分子機構解析
連絡先：〒769-2193 香川県さぬき市志度1314-1
E-mail: tominagat@kph.bunri-u.ac.jp
冨永洋子（とみなが　ようこ）
徳島文理大学香川薬学部技術補佐員
富士通，理化学研究所脳科学総合研究センターテクニカルスタッフなどを経て現職．
研究内容：光計測を使った脳機能解析

Saito *et al. Molecular Brain* 2010, **3**:40
http://www.molecularbrain.com/content/3/1/40

Molecular Brain

RESEARCH **Open Access**

The physiological roles of vesicular GABA transporter during embryonic development: a study using knockout mice

Kenzi Saito[1,2], Toshikazu Kakizaki[1,3], Ryotaro Hayashi[4], Hiroshi Nishimaru[5], Tomonori Furukawa[6], Yoichi Nakazato[7], Shigeo Takamori[8], Satoe Ebihara[9], Masakazu Uematsu[10], Masayoshi Mishina[11], Jun-ichi Miyazaki[12], Minesuke Yokoyama[13], Shiro Konishi[13], Koichi Inoue[6], Atsuo Fukuda[6], Manabu Fukumoto[4], Kenji Nakamura[13], Kunihiko Obata[14], Yuchio Yanagawa[1,3*]

Abstract

Background: The vesicular GABA transporter (VGAT) loads GABA and glycine from the neuronal cytoplasm into synaptic vesicles. To address functional importance of VGAT during embryonic development, we generated global VGAT knockout mice and analyzed them.

Results: VGAT knockouts at embryonic day (E) 18.5 exhibited substantial increases in overall GABA and glycine, but not glutamate, contents in the forebrain. Electrophysiological recordings from E17.5-18.5 spinal cord motoneurons demonstrated that VGAT knockouts presented no spontaneous inhibitory postsynaptic currents mediated by GABA and glycine. Histological examination of E18.5 knockout fetuses revealed reductions in the trapezius muscle, hepatic congestion and little alveolar spaces in the lung, indicating that the development of skeletal muscle, liver and lung in these mice was severely affected.

Conclusion: VGAT is fundamental for the GABA- and/or glycine-mediated transmission that supports embryonic development. VGAT knockout mice will be useful for further investigating the roles of VGAT in normal physiology and pathophysiologic processes.

Background

GABAergic and glycinergic neurotransmissions play critical roles in the central nervous system (CNS), because they regulate network activity and are essential for a number of brain functions, such as cognition, perception, movement and respiration. In the adult mammalian CNS, GABA and glycine are the main inhibitory neurotransmitters, but in fetal life and early postnatal development, both neurotransmitters act as either excitatory or inhibitory, depending on the intracellular chloride concentration.

GABA is synthesized from glutamic acid by glutamate decarboxylase (GAD) [1] and is accumulated into synaptic vesicles by the vesicular GABA transporter (VGAT) [2,3]. Two isozymes of GAD, GAD65 and GAD67, are primarily expressed in GABAergic neurons [4,5]. GAD65 knockout mice exhibit spontaneous seizures, elevated anxiety and altered sensitivity to pain [6,7]. GAD67 knockout mice die of cleft palate at birth [8]. VGAT is present in both GABAergic and glycinergic neurons and is also called the vesicular inhibitory amino acid transporter (VIAAT) [3,9]. In addition to its presence at GABAergic and glycinergic synapses, the role of VGAT/VIAAT in GABA and glycine release is supported by electrophysiological evidence from primary cultured hippocampal or spinal cord neurons of VGAT knockout mice [10] and VGAT-transfected secretory cells [11]. VGAT knockout mice die perinatally and show a hunched posture, cleft palate and omphalocele [10].

Divergent roles for the VGAT proteins are implicated in the nervous system. However, the contribution of

---

* Correspondence: yanagawa@med.gunma-u.ac.jp
[1] Department of Genetic and Behavioral Neuroscience, Gunma University Graduate School of Medicine, Maebashi 371-8511, Japan
Full list of author information is available at the end of the article

VGAT to tissues or cells outside of the CNS remains largely unclear. For example, neither muscle, lung nor liver phenotypes have been reported for these knockout mice. We independently generated VGAT knockout mice. To further investigate the roles of VGAT during development, we performed histopathological analyses in VGAT knockout muscle, lung and liver at an embryonic stage. These mice showed a reduction in the trapezius muscles, smaller saccules in the lung, and congestion in the liver. In addition, in VGAT knockout spinal cord motoneurons (MNs), spontaneous inhibitory postsynaptic currents (IPSCs) were absent. These experiments indicate that VGAT has an important role in the GABA- and/or glycine-mediated transmission that supports life. Preliminary results have been published in an abstract form [12].

Results

Generation of VGAT$^{-/-}$ mice

The targeting strategy used for the generation of VGAT knockout mice is shown in Figure 1A. Exons 2 and 3 encode the putative ten-transmembrane domain and C-terminus of the VGAT protein [3,13], and accordingly, the deletion of these regions was expected to destroy the function of the VGAT protein. Correctly targeted ES cell clones isolated were microinjected into blastocysts to generate chimeric mice. These mice were then crossed with C57BL/6 mice to generate heterozygous mice carrying one floxneo allele (VGAT$^{floxneo/+}$ mice).

We generated the VGAT knockout allele by crossing VGAT$^{floxneo/+}$ mice with CAG-Cre mice, in which Cre recombinase is expressed ubiquitously [14]. Genotyping was performed by Southern blot analysis (Figure 1B) and PCR (Figure 1C), and the DNA sequences around the loxP site in the knockout allele were also confirmed (data not shown). To obtain homozygous VGAT knockout (VGAT$^{-/-}$) mice, we intercrossed the VGAT$^{+/-}$ mice. Western blot analysis revealed no VGAT protein expression in embryonic day (E) 18.5 VGAT$^{-/-}$ brain, whereas VGAT protein expression in VGAT$^{+/-}$ mouse brains was reduced to about half of the wild-type level (Figure 1D). All E18.5 VGAT$^{-/-}$ fetuses displayed cleft palate (Figure 1E) and omphalocele (Figure 1F), phenotypes that are consistent with those described by Wojcik et al. [10].

No VGAT$^{-/-}$ mice survived beyond birth (Table 1). To estimate the time of death of VGAT$^{-/-}$ mice, we performed timed matings of the VGAT$^{+/-}$ mice and obtained the fetuses via cesarean section. Among the E18.5 offspring derived from the intercrosses of VGAT$^{+/-}$ mice, VGAT$^{-/-}$ fetuses were obtained at the expected Mendelian ratio (27.3%, 77 VGAT$^{-/-}$ of 282 littermates) and more than 97% of them (75 of 77) were alive (judged by their umbilical beats or heartbeats, Table 1). When delivered by cesarean section on E18.5, both VGAT$^{+/+}$ (7 of 7) and VGAT$^{+/-}$ (11 of 12) fetuses began respiration, but none of the VGAT$^{-/-}$ fetuses (n = 7) began to breathe. Therefore, it is probable that VGAT$^{-/-}$ mice died at birth due to respiratory failure.

Elevations in GABA and glycine contents in VGAT$^{-/-}$ forebrains

In the absence of vesicular storage, neurotransmitter levels can be altered, and this alteration depends on the absence of the vesicular transporter. For example, monoamines are drastically reduced in vesicular monoamine transporter 2 knockout brains [15], but acetylcholine (ACh) is increased in vesicular acetylcholine transporter (VAChT) knockout brains compared to control wild-type brains [16]. Therefore, we measured the amount of the neurotransmitters, GABA, glycine and glutamate in E18.5 VGAT$^{-/-}$ forebrain by HPLC. As shown in Figure 2A, VGAT$^{-/-}$ fetuses showed significant increases in both GABA and glycine, but not glutamate, compared to VGAT$^{+/+}$ fetuses. It is possible that the increase in GABA content in VGAT$^{-/-}$ fetuses was due to the elevated expression levels of GABA-synthesizing enzymes. To test for this possibility, we analyzed the expression levels of GAD65 and GAD67 in the embryonic brains. Our Western blot analysis showed that the expression levels of both GAD65 and GAD67 in VGAT$^{+/+}$ and VGAT$^{-/-}$ brains were similar (Figure 2B). These results indicate that the increase in GABA content was not derived from elevated amounts of GABA-synthesizing enzymes in VGAT$^{-/-}$ embryos.

Absence of functional inhibitory synaptic transmission in the VGAT$^{-/-}$ spinal cord

To examine the physiological nature of synaptic inputs to spinal MNs, we performed whole-cell patch-clamp recordings using isolated spinal cord preparations taken from VGAT$^{-/-}$ and control mouse embryos. In these preparations, the neuronal connections within the spinal cord are kept relatively intact [17]. In control lumbar MNs, spontaneous outward currents were observed when the membrane potential was depolarized at -40 mV above the chloride ion reversal potential (approximately -78 mV in the present experimental condition). These currents were blocked by bath application of the glycinergic antagonist strychnine and the GABAergic antagonist picrotoxin, indicating that the currents were IPSCs (n = 8, Figure 3A). In contrast, we did not detect such spontaneous IPSCs in VGAT$^{-/-}$ MNs (n = 12, Figure 3B). When the membrane potential was held at -70 mV, spontaneous inward currents were observed both in control and VGAT$^{-/-}$ MNs (Figure 3A and 3B). These inward currents were abolished by the concomitant bath application of the ionotropic

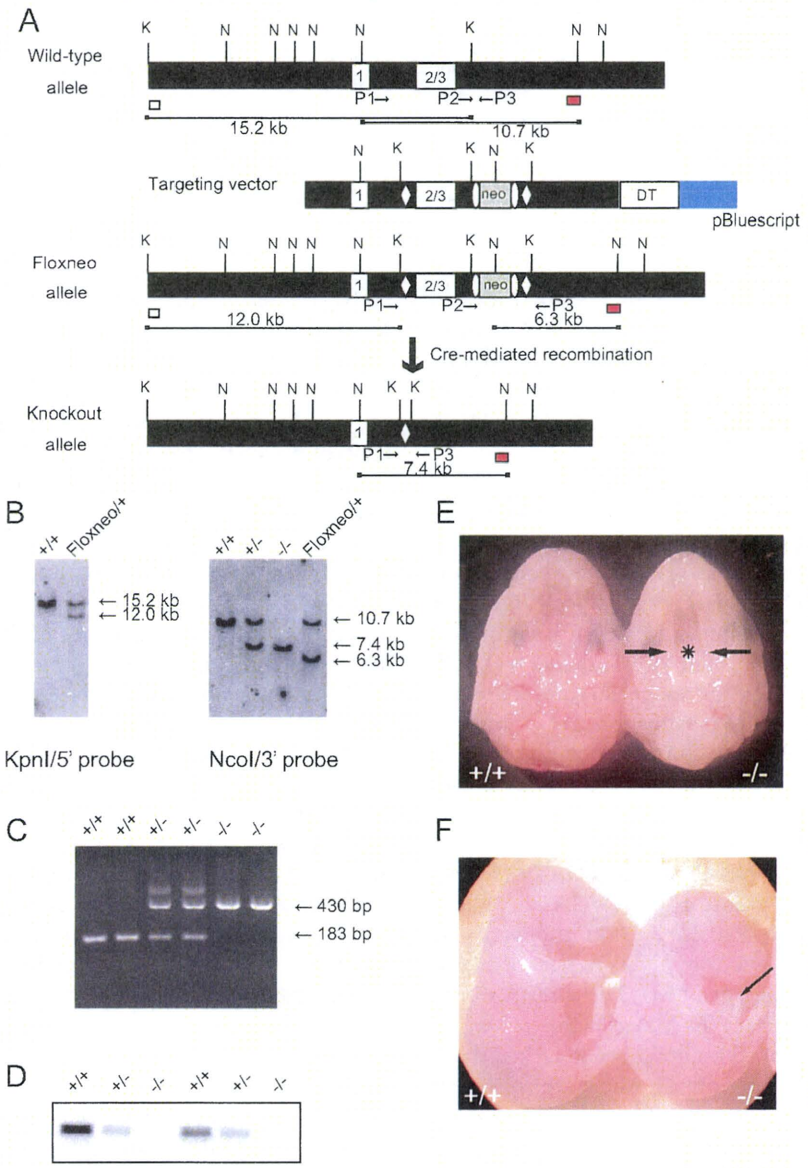

Figure 1 Generation of VGAT$^{-/-}$ mice. (A) Schematic representation of the wild-type VGAT allele, the targeting vector, the VGAT-floxneo allele, and the VGAT knockout allele. Exons are represented by numbered white boxes. LoxP sites (open diamonds) and a PGK-Neo cassette (neo; gray box) flanked by the frt sites (open ellipses) were introduced into the wild-type VGAT locus by homologous recombination to produce the floxneo allele. The probes used for Southern blot analysis are indicated as white (5' probe) and red (3' probe) boxes. The expected sizes of the KpnI- and NcoI-digested genomic DNA fragments hybridized with the 5' and 3' probes, respectively, are indicated as lines under the schemes. Relevant restriction sites are indicated as follows: K, KpnI; N, NcoI. PCR primers are indicated as arrows. (B) (Left) Southern blot analysis of KpnI-digested genomic DNA isolated from VGAT$^{+/+}$ (+/+) and VGAT$^{floxneo/+}$ (Floxneo/+) mice using the 5' probe indicated in A. The wild-type allele corresponds to the 15.2 kb band, whereas the floxneo allele corresponds to the 12.0 kb band. (Right) Southern blot analysis of NcoI-digested genomic DNA isolated from VGAT$^{+/+}$ (+/+), VGAT$^{+/-}$ (+/-), VGAT$^{-/-}$ (-/-), and VGAT$^{floxneo/+}$ (Floxneo/+) mice using the 3' probe indicated in A. The wild-type allele, the knockout allele, and the floxneo allele correspond to the 10.7 kb, 7.4 kb, and 6.3 kb bands, respectively. (C) Genotyping of offspring from intercrosses of VGAT$^{+/-}$ mice by PCR. Three primers were used (see Methods). Primers P2 and P3 produce a 183 bp fragment that represents the wild-type allele, whereas primers P1 and P3 produce a 430 bp fragment that represents the knockout allele. (D) Western blot analysis of E18.5 whole brain homogenates from VGAT$^{+/+}$ (+/+), VGAT$^{+/-}$ (+/-), VGAT$^{-/-}$ (-/-) using the anti-VGAT antibody directed against an N-terminal epitope. (E) Ventral views of the upper jaw of E18.5 VGAT$^{+/+}$ (+/+) and VGAT$^{-/-}$ (-/-) mice. In contrast to the completely fused palate of a VGAT$^{+/+}$ mouse, secondary palatal shelves of a VGAT$^{-/-}$ mouse did not contact each other (arrows), and its nasal cavity (asterisk) could be seen. (F) Lateral views of E18.5 VGAT$^{+/+}$ (+/+) and VGAT$^{-/-}$ (-/-) mice. An arrow indicates omphalocele in a VGAT$^{-/-}$ mouse. In addition, the VGAT$^{-/-}$ mouse showed an extremely hunched position in contrast to the VGAT$^{+/+}$ mouse.

Table 1 Genotypes of offspring from intercrosses of VGAT $^{+/-}$ mice and phenotypes of VGAT $^{-/-}$ mice

Age	Genotype			Phenotype		
	+/+	+/-	-/-	No. of -/- found dead	No. of -/- with omphalocele	No. of -/- with cleft palate
E18.5	69 (24.5%)	136 (48.2%)	77 (27.3%)	2/77*	77/77*	29/29*
Newborn	22 (19.6%)	76 (67.9%)	14 (12.5%)	14/14*	Not determined	Not determined

*affected/examined.

glutamate receptor blockers, a non-NMDA receptor antagonist 6-cyano-7-nitroquinoxaline-2,3-dione (CNQX) and an NMDA receptor antagonist D-2-amino-5-phosphonovaleric acid (AP5), indicating that MNs received excitatory synaptic transmission in the VGAT$^{-/-}$ spinal cord.

Alterations in body weight, response to stimuli, trapezius muscle, liver and lung of VGAT$^{-/-}$ mice

Wojcik et al. [10] reported that VGAT$^{-/-}$ mice display the phenotypes such as cleft palate, omphalocele, hunched posture, immobility and stiffness. However, we proposed that there would be some other alterations in VGAT$^{-/-}$ mice because VGAT is an essential molecule for GABAergic and glycinergic transmission. To address the question whether VGAT is essential for fetal growth, we initially measured the body weight of VGAT$^{-/-}$ fetuses compared to VGAT$^{+/+}$ and VGAT$^{+/-}$ littermates. The body weight of the E18.5 VGAT$^{-/-}$ fetuses was significantly lower than that of VGAT$^{+/+}$ and VGAT$^{+/-}$ fetuses (VGAT$^{+/+}$: 1.18 ± 0.11 grams, n = 17; VGAT$^{+/-}$: 1.20 ± 0.08 grams, n = 45; VGAT$^{-/-}$: 1.05 ± 0.11 grams, n = 32 [mean ± SD], $P < 0.001$, one-way ANOVA, post hoc Fisher's least significant difference test). These results indicate that VGAT is important for fetal growth.

VGAT$^{-/-}$ fetuses exhibited immobility and lacked spontaneous limb and body movements, which are consistent with a report by Wojcik et al. [10]. To further address the question of whether the lack of movement in VGAT$^{-/-}$ fetuses was restricted to a defect in spontaneous movement, we examined the response of E18.5 VGAT$^{-/-}$ fetuses to mechanical stimuli. VGAT$^{+/+}$, VGAT$^{+/-}$ and VGAT$^{-/-}$ fetuses were obtained via cesarean section and maintained alive in phosphate buffered saline. None of the VGAT$^{-/-}$ fetuses (n = 16) responded to a pinch of the tail by forceps, but all VGAT$^{+/+}$ (n = 16) and VGAT$^{+/-}$ (n = 53) fetuses responded with a twisting of the trunk. These results suggest that VGAT$^{-/-}$ fetuses suffer from severe impairments in motor function.

Because the hunched posture observed in VGAT$^{-/-}$ mice (Figure 1F) suggested defects in skeletal muscles or bones [18,19], we performed a histological examination of skeletal muscles and bones in the E18.5 embryos. Trapezius muscle was thinner in VGAT$^{-/-}$ mice than in the control mice (Figure 4A, B). The VGAT$^{-/-}$ ribs in the lower part were depressed, and their position was retracted toward the inside compared to control (Figure 4C, D). Furthermore, the spaces between each rib appeared narrower in VGAT$^{-/-}$ mice compared to the control mice (Figure 4C, D). Abdominal organs were examined histologically in an attempt to identify pathological findings associated with defects in VGAT$^{-/-}$ mice. Not only omphalocele (Figure 1F) but also hepatic congestion were characteristic of VGAT$^{-/-}$ embryos (Figure 4E, F). These results suggest that the crouching posture caused by an imbalance of the strength between the dorsal and ventral muscles made the thorax expand ineffectively, leading to an increase in intra-abdominal pressure in VGAT$^{-/-}$ embryos. Although omphalocele can be caused by a malformation of the ventral body wall [20], the rectus abdominis muscle showed no apparent abnormality in VGAT$^{-/-}$ mice (data not shown).

The VGAT$^{-/-}$ mice lacked autonomous and joggling-induced breathing movements, consistent with the report by Fujii et al. [21]. However, there is still uncertainty regarding the mechanism responsible for the respiratory failure caused by the loss of VGAT protein. To understand the pathology causing respiratory failure in VGAT$^{-/-}$ mice, we fixed embryos at E18.5, the day prior to birth, and performed pathohistology of the lungs. Examination under a microscope revealed that the VGAT$^{-/-}$ lung barely contained alveolar spaces compared to the control lung (Figure 4G, H). A possible cause of atelectasis was reported defect in the diaphragm [22]. We examined the VGAT$^{-/-}$ diaphragm histologically, but we didn't detect any difference in the diaphragm between the VGAT$^{-/-}$ and control mice.

The alterations in the VGAT$^{-/-}$ muscle, liver and lung were likely caused by the loss of VGAT in the CNS, but not the loss of VGAT in the peripheral tissue because VGAT transcripts were detected in brain and spinal cord, but not in muscle, liver or lung [2,3].

Comparison of cleft palate and omphalocele between VGAT$^{-/-}$ mice and GAD67$^{-/-}$ mice

Cleft palate is exhibited by VGAT$^{-/-}$ and GAD67$^{-/-}$ mice [8,10,23], demonstrating that GABAergic transmissions are involved in palatogenesis. Because VGAT and